



## BIROn - Birkbeck Institutional Research Online

Pogge von Strandmann, Philip A.E. and Frings, P.J. and Murphy, M.J. (2017) Lithium isotope behaviour during weathering in the Ganges Alluvial Plain. *Geochimica et Cosmochimica Acta* 198 , pp. 17-31. ISSN 0016-7037.

Downloaded from: <https://eprints.bbk.ac.uk/id/eprint/17901/>

*Usage Guidelines:*

Please refer to usage guidelines at <https://eprints.bbk.ac.uk/policies.html> or alternatively contact [lib-eprints@bbk.ac.uk](mailto:lib-eprints@bbk.ac.uk).

1 **Lithium isotope behaviour during weathering in the Ganges alluvial plain**

2

3 Philip A.E. Pogge von Strandmann<sup>1\*</sup>, Patrick J. Frings<sup>2,3</sup>, Melissa J. Murphy<sup>4</sup>

4

5 <sup>1</sup>London Geochemistry and Isotope centre (LOGIC), Institute of Earth and

6 Planetary Sciences, University College London and Birkbeck, University of

7 London, Gower Street, London, WC1E 6BT, UK.

8 <sup>2</sup>Earth Surface Geochemistry, Helmholtz Centre Potsdam, GFZ German Research

9 Centre for Geosciences, Telegraphenberg, 14473 Potsdam, Germany.

10 <sup>3</sup>Department of Geoscience, Swedish Museum of Natural History, 10405

11 Stockholm, Sweden.

12 <sup>4</sup>Department of Earth Sciences, Oxford University, South Parks Road, Oxford, OX1

13 3AN, UK.

14

15 \*Corresponding author: p.strandmann@ucl.ac.uk

16

17 Abstract

18 The Ganges river system is responsible for the transportation of a large flux of

19 dissolved materials derived from Himalayan weathering to the oceans. Silicate

20 weathering-driven cooling resulting from uplift of the Himalayas has been

21 proposed to be a key player in Cenozoic climate variation. This study has

22 analysed Li isotope ( $\delta^7\text{Li}$ ) ratios from over 50 Ganges river waters and

23 sediments, in order to trace silicate weathering processes. Sediments have  $\delta^7\text{Li}$  of

24  $\sim 0\text{‰}$ , identical to bulk continental crust, however suspended sediment depth

25 profiles do not display variations associated with grain size that have been

26 observed in other large river systems. Dissolved  $\delta^7\text{Li}$  are low ( $\sim 11\text{‰}$ ) in the  
27 Ganges headwaters, but reach a constant value of  $21 \pm 1.6\text{‰}$  within a relatively  
28 short distance downstream, which is then maintained for almost 2000 km to the  
29 Ganges mouth. Given that Li isotopes are controlled by the ratio of primary  
30 mineral dissolution to secondary mineral formation, this suggests that the  
31 Ganges floodplain is at steady-state in terms of these processes for most of its  
32 length. Low  $\delta^7\text{Li}$  in the mountainous regions suggest silicate weathering is  
33 therefore at its most congruent where uplift and fresh silicate exposure rates are  
34 high. However, there is no correlation between  $\delta^7\text{Li}$  and the silicate weathering  
35 rate in these rivers, suggesting that Li isotopes cannot be used as a weathering-  
36 rate tracer, although they do inform on weathering congruency and intensity.  
37 The close-to-constant  $\delta^7\text{Li}$  values for the final 2000 km of Ganges flow also  
38 suggest that once the size of the alluvial plain reached more than  $\sim 500$  km (the  
39 flow distance after which riverine  $\delta^7\text{Li}$  stops varying), the Ganges exerted little  
40 influence on the changing Cenozoic seawater  $\delta^7\text{Li}$ , because riverine  $\delta^7\text{Li}$  attained  
41 a near steady-state composition.

42

43

#### 44 1.0 Introduction

45 Chemical weathering of silicate rocks is a significant long-term removal  
46 process of atmospheric  $\text{CO}_2$ , both through supply of cations and alkalinity for  
47 marine carbonate precipitation, and through supply of nutrients for organic  
48 carbon burial (Berner, 2003; Berner et al., 1983; Walker et al., 1981; West et al.,  
49 2002; West et al., 2005). As such, it has long been postulated as a key long-term  
50 climate control and stabilisation mechanism. In the Cenozoic, in particular, it is

51 questioned whether the observed ~40 Myr cooling trend and CO<sub>2</sub> decline were  
52 caused by uplift of the Himalayas, which increased the supply of primary  
53 material for weathering, which in turn removed more atmospheric CO<sub>2</sub> (Raymo,  
54 1994; Raymo and Ruddiman, 1992; Raymo et al., 1988). The question of whether  
55 tectonic processes can strongly affect CO<sub>2</sub> drawdown is critical for  
56 understanding the Earth's climate system, because it may suggest that a  
57 temperature-driven stabilising feedback on CO<sub>2</sub> via weathering (the Earth's  
58 "weathering thermostat") is at times a relatively weak control on climate  
59 compared to a supply-driven or organic carbon-driven control (Gíslason et al.,  
60 2006; Gíslason et al., 2009; Maher and Chamberlain, 2014; Oelkers et al., 2012;  
61 West, 2012).

62 Evidence for the controls on weathering initially focussed on marine Sr  
63 isotope ratios, which started to increase approximately 40 Ma ago (McArthur et  
64 al., 2001). This increase was interpreted as a greater input of radiogenic  
65 continental material, implying greater weathering and CO<sub>2</sub> drawdown, likely due  
66 to Himalayan uplift. However, it has since become clear that the interpretation of  
67 the <sup>87</sup>Sr/<sup>86</sup>Sr curve is not straightforward, because of the effect of  
68 metamorphosed radiogenic Himalayan carbonates (Bickle et al., 2005; Galy et al.,  
69 1999; Oliver et al., 2003; Palmer and Edmond, 1992). It is therefore not clear  
70 how much of the increase in seawater <sup>87</sup>Sr/<sup>86</sup>Sr is due to weathering of  
71 continental silicates, and how much due to metamorphosed carbonates (Galy et  
72 al., 1999), the latter of which would not affect atmospheric CO<sub>2</sub> on timescales  
73 >~10,000 years, and may even be a source of CO<sub>2</sub>, if the dominant source of  
74 acidity is sulphuric acid (Torres et al., 2014). Equally, seawater osmium isotopes  
75 show a punctuated increase from ~60 Ma (Peucker-Ehrenbrink and Ravizza,

76 2000; Peucker-Ehrenbrink et al., 1995), and here debate has focussed on the  
77 control radiogenic black shales in Himalayan lithologies may exert on seawater  
78  $^{187}\text{Os}/^{188}\text{Os}$  ratios (Pierson-Wickmann et al., 2002a, b). Hence, both of the above  
79 radiogenic isotope systems can at best only provide somewhat ambiguous  
80 interpretations as to whether weathering rates, or rock weatherability, increased  
81 due to the Himalayas, because of the effect of individual Sr- and Os-rich  
82 lithologies.

83 More recently, lithium isotopes have been used to try to answer this  
84 question. Seawater  $\delta^7\text{Li}$  appears to have started increasing between 50 and 60  
85 Ma, with behaviour more similar to Os than Sr isotope records (Hathorne and  
86 James, 2006; Misra and Froelich, 2012). As a stable isotope system, Li is virtually  
87 unaffected by the lithologies undergoing weathering, and is isotopically  
88 fractionated by the weathering process. Specifically, Li in rocks is  
89 overwhelmingly dominated by the silicate fraction, meaning that Li isotopes are  
90 probably the only proxy that solely traces silicate weathering (Kisakürek et al.,  
91 2005; Millot et al., 2010). The Li isotope ratio of silicate rocks describes a very  
92 narrow range ( $\delta^7\text{Li}_{\text{continental crust}} \sim 0.6 \pm 0.6\text{‰}$  (Sauzeat et al., 2015; Teng et al.,  
93 2004);  $\delta^7\text{Li}_{\text{basalt}} = \sim 3\text{--}5\text{‰}$  (Elliott et al., 2006; Tomascak et al., 2008)), relative to  
94 that reported in river waters ( $\delta^7\text{Li} = 2\text{--}44\text{‰}$ ; global mean  $23\text{‰}$  (Bagard et al.,  
95 2015; Dellinger et al., 2014; Henchiri et al., 2016; Huh et al., 2001; Huh et al.,  
96 1998; Kisakürek et al., 2005; Liu et al., 2015; Millot et al., 2010; Pogge von  
97 Strandmann et al., 2010; Pogge von Strandmann et al., 2006; Pogge von  
98 Strandmann and Henderson, 2015; Rad et al., 2013; Vigier et al., 2009; Wang et  
99 al., 2015; Wimpenny et al., 2010b; Witherow et al., 2010). This high variability in  
100 rivers is caused by weathering processes: dissolution of silicates causes no

101 isotope fractionation, but secondary minerals formed during weathering  
102 preferentially take up  $^6\text{Li}$ , driving residual waters isotopically heavy (Huh et al.,  
103 2001; Pistiner and Henderson, 2003; Pogge von Strandmann et al., 2010; Vigier  
104 et al., 2008; Wimpenny et al., 2010a). Therefore, surface water  $\delta^7\text{Li}$  is controlled  
105 by the ratio of primary mineral dissolution (low  $\delta^7\text{Li}$ , high [Li]) relative to  
106 secondary mineral formation (driving waters to high  $\delta^7\text{Li}$ , and low [Li]). This  
107 ratio has also been described as the weathering congruency (Misra and Froelich,  
108 2012; Pogge von Strandmann et al., 2013), weathering efficiency (Pogge von  
109 Strandmann and Henderson, 2015) or weathering intensity (Dellinger et al.,  
110 2015; Pogge von Strandmann et al., 2010). When riverine  $\delta^7\text{Li}$  = rock  $\delta^7\text{Li}$ , then  
111 weathering is congruent (water chemistry = rock chemistry), efficient (cations  
112 are not retained in clays, but are delivered to the oceans) and low intensity (little  
113 clay formation, and a low weathering to denudation ratio – bearing in mind that  
114 “weathering intensity” has been defined differently by different authors).

115         If, as seems likely, the  $\sim 9\%$  increase from early Cenozoic seawater to  
116 the present day was controlled by changes in weathering rates or processes, it  
117 would imply an increasing relative proportion of secondary mineral formation  
118 (Bouchez et al., 2013; Li and West, 2014; Misra and Froelich, 2012; Vigier and  
119 Godderis, 2015; Wanner et al., 2014). Initially, this was interpreted as directly  
120 due to mountain uplift (Misra and Froelich, 2012). However, High Himalayan  
121 rivers tend to have low  $\delta^7\text{Li}$  values suggesting little clay formation (Kisakürek et  
122 al., 2005), and in general uplifting and denuding terrains tend to have lower  $\delta^7\text{Li}$   
123 than flatter terrains, because of the continuous exposure of isotopically light  
124 primary rock, and lower rock-water interaction times in the former, and longer  
125 water-rock interaction times leading to greater precipitation of secondary

126 minerals in the low-lying areas (Dellinger et al., 2015; Pogge von Strandmann  
127 and Henderson, 2015). This has led to the proposal that the seawater  $\delta^7\text{Li}$  curve  
128 is charting the evolution of the Himalayan floodplains (or others, such as those of  
129 the Andes), rather than the mountain uplift and exposure itself (Pogge von  
130 Strandmann and Henderson, 2015). This also agrees with the concept that more  
131  $\text{CO}_2$  is drawn down in these floodplains, rather than in the mountains (Lupker et  
132 al., 2012; West et al., 2002).

133           Therefore, studies have begun examining the Ganges-Brahmaputra  
134 floodplains to examine weathering and Li behaviour in low-lying floodplain  
135 settings. Sample sets taken  $\sim 10$  years apart (in the late 1980s and late 1990s)  
136 from Rishikesh in the Ganges headwaters have lower  $\delta^7\text{Li}$  than samples taken  
137 close to the river mouth (Bagard et al., 2015; Huh et al., 1998). To date, the  
138 highest sample resolution is from Bagard et al. (2015), which comprises four  
139 samples along the  $\sim 2500$  km of the Ganges, with  $\delta^7\text{Li}$  increasing from  $\sim 10$  to  
140 24‰.

141           This study has increased this sample resolution by an order of  
142 magnitude, with an average sample spacing of  $\sim 50$  km along the Ganges and its  
143 tributaries, using samples that have previously been analysed for silicon isotopes  
144 (Frings et al., 2015). We have also analysed the Li isotope composition of a series  
145 of sediments and suspended load material from various parts of the Ganges  
146 plain, which has not previously been attempted in this region. In combination  
147 with published data from the High Himalayas, and the above-mentioned low  
148 sample-resolution studies, we provide an insight into how the Ganges-  
149 Brahmaputra floodplain affects Li isotope signals discharging into the ocean, and

150 what this tells us about modern floodplain weathering and global weathering  
151 signals in the geological past.

152

### 153 2.0 Samples

154 The study area and samples are described by Frings et al. (2015), and  
155 focus on the Ganges Alluvial Plain. Briefly, the Ganges (Fig. 1) drains a basin of  
156  $\sim 0.98 \times 10^6 \text{ km}^2$  and has a mean annual discharge in Bangladesh of  $\sim 490 \times 10^9$   
157  $\text{m}^3 \text{ yr}^{-1}$ . The drainage area covers the Himalayas to the north, the hills of the  
158 Indian peninsular to the south, and the Ganges Alluvial Plain between them (Fig.  
159 1). 80% of water in the drainage area is provided during the summer monsoon.  
160 Sampling occurred at the end of the peak flood, in September 2013, and samples  
161 were taken from 51 locations from tributaries around Rishikesh in NW India, at  
162 the base of the Himalayas, along the Ganges and tributaries, to Farrakah, which is  
163 where the Ganges distributary system begins. A further sample was taken close  
164 to Calcutta, along the Hooghly River, which is one of these distributaries draining  
165 into the Bay of Bengal. Overall the Ganges Basin has been extensively studied for  
166 weathering processes, with a particular emphasis on the Himalayan portion of  
167 the system (Bickle et al., 2005; Dalai et al., 2002; Galy and France-Lanord, 1999;  
168 Galy et al., 1999; Rai et al., 2010).

169

### 170 3.0 Methods

171 Samples were collected in 2013 as detailed by Frings et al. (2015). At  
172 most locations, water depth was determined with a ballasted sounding line, and  
173 5 litres of water collected at the surface, at maximum depth, and at the centre  
174 point using a horizontal van Dorn style water sampler. This was filtered at 0.4



175  $\mu\text{m}$  within a few hours using a Teflon-coated pressure filtration system. The  
176 filters were retained, freeze-dried and the sediment gently removed from the  
177 filter.

178 Anion concentrations were measured by ion chromatography at the  
179 Department of Biology, Lund University, while major and minor cations,  
180 including Li, were measured by ICP-OES and ICP-MS, respectively, at University  
181 College London. The precision of these measurements is  $<\pm 5\%$  (Frings et al.,  
182 2015). Sediments and rock standards were dissolved in steps of HF-HNO<sub>3</sub>,  
183 followed by HNO<sub>3</sub> and HCl.

184 For Li isotope analysis, sufficient sample was dried down to attain  $\sim 20\text{ng}$   
185 of Li, and passed through a two-step cation exchange chromatography (AG50W  
186 X-12), using dilute HCl as an eluent. Isotopic analyses were conducted on a Nu  
187 Instruments HR multi-collector ICP-MS, relative to the standard L-SVEC (Flesch  
188 et al., 1973), at the Department of Earth Sciences, Oxford University. The exact  
189 methods for chemistry and analysis are detailed elsewhere (Pogge von  
190 Strandmann et al., 2011; Pogge von Strandmann and Henderson, 2015; Pogge  
191 von Strandmann et al., 2013). Seawater was run as an “unknown” standard,  
192 yielding  $\delta^7\text{Li} = 31.3 \pm 0.6\text{‰}$  (2sd, n=48, column passes=48) over a three-year  
193 period. Two rock standards were also run, granite JG-2 ( $\delta^7\text{Li} = 0.4 \pm 0.2\text{‰}$ , n=3)  
194 and Wyoming oil shale SGR-1b ( $\delta^7\text{Li} = 3.6 \pm 0.4\text{‰}$ , n=3), where results are within  
195 uncertainty of other published values (Jeffcoate et al., 2004; Phan et al., 2016;  
196 Vigier et al., 2008; Wunder et al., 2006). The total procedural blank of this  
197 method was effectively undetectable ( $<0.005\text{ng Li}$ ), which is insignificant relative  
198 to the 10–20 ng of Li analysed in each sample.

199

## 200 4.0 Results

201 Overall, the sampled rivers exhibit a standard positive trend between  
202 Ca/Na and Mg/Na (not shown), and exhibit a broadly similar range to that  
203 displayed by global rivers (Gaillardet et al., 1999b). Most samples are closer to  
204 the lower, silicate, end-member.

205 Lithium concentrations in the river waters vary between 0.4 and 11.7  
206 ng/ml (Table 1). This is a similar range to other large multi-lithology rivers  
207 systems that have been studied, such as the Mackenzie River (Millot et al., 2010)  
208 and the Amazon (Dellinger et al., 2015). Highest [Li] in these river samples are in  
209 the Yamuna River, but concentrations decrease in the Yamuna before it joins the  
210 Ganges, and therefore at the confluence of the two rivers, [Li] in both is broadly  
211 similar. Lowest [Li] occurs in the Ganges at the base of the Himalayas, and also in  
212 all rivers within ~1000km of the river mouth, within the lower reaches of the  
213 alluvial plain (Fig. 2a).

214 Li isotope ratios range between 10.7 and 24.8‰, with the bulk of the data  
215 clustered in a relatively narrow band between 19 and 22‰. This is a narrower  
216 range than the Mackenzie and Amazon river systems overall (9–29‰ and 1.2–  
217 33‰, respectively), but greater than the Mackenzie lowland regions (10–17‰)  
218 (Dellinger et al., 2015; Millot et al., 2010). The Ganges itself has the lowest  $\delta^7\text{Li}$  in  
219 the Himalayan foothills (10.7–12.9‰; Fig. 2b). At a similar distance upstream,  
220 the Yamuna has a much higher  $\delta^7\text{Li}$  (18–22‰), highlighting the difference  
221 between alluvial plain and foothills weathering. From ~2000km upstream of the  
222 river mouth,  $\delta^7\text{Li}$  values are fairly constant at  $\delta^7\text{Li} = 21 \pm 1.6\text{‰}$ . Thus, rivers  
223 wholly draining the alluvial plain have virtually identical  $\delta^7\text{Li}$  to the downstream  
224 Ganges. Unlike data reported from the Congo (Henchiri et al., 2016), Li data from

225 the Ganges do not appear represent simple two-endmember mixing, but imply  
226 isotope fractionation processes occurring during weathering (Section 5.1).

227 River sediment Li isotope ratios range from -2.6 to 2.9‰, with an average  
228  $\delta^7\text{Li}$  of  $-0.3 \pm 1.3\text{‰}$  (Table 2), which is within uncertainty of the value of the  
229 upper continental crust (Sauzeat et al., 2015; Teng et al., 2004), although they  
230 exhibit a larger range than values of -1.02 to +0.39‰ reported from a single  
231 location close to the mouth of the Ganges (Dellinger et al., 2014). Given that  
232 rivers such as the Amazon have displayed depth-trends in Li isotope  
233 composition, with decreasing  $\delta^7\text{Li}$  values with increasing grain size (Dellinger et  
234 al., 2014), this study analysed  $\delta^7\text{Li}$  values from sediments at different depths in  
235 several locations, as well as from a bank deposit. No trend with depth exists in  
236 these rivers, implying that the suspended load is better mixed, or has a more  
237 consistent mineralogy, than in the Amazon. Overall the 4.5‰ range in sediment  
238 isotope ratios over ~2000 km of river flow (Fig. 3) is similar to the 5‰ range in  
239 the Mackenzie River basin (Millot et al., 2010), but smaller than the 9‰ range  
240 reported from the Amazon (Dellinger et al., 2014).

241

## 242 5.0 Discussion

243 Lithium isotopes provide information on the balance of silicate rock  
244 dissolution to secondary mineral formation, described as the weathering  
245 congruency, or the weathering intensity. It is important to note that different  
246 studies define “weathering intensity” in different ways, such that high  
247 weathering intensity has been considered as high primary rock dissolution and  
248 low dissolved  $\delta^7\text{Li}$  (Kisakürek et al., 2005; Pogge von Strandmann et al., 2010;  
249 Pogge von Strandmann et al., 2013), while in other studies it is considered as

250 high secondary mineral formation and high dissolved  $\delta^7\text{Li}$  (Dellinger et al., 2015).  
251 In this study we adopt the terminology of Dellinger et al., 2015, while noting that  
252 yet other definitions are also available (Millot et al., 2010). All of these studies  
253 however agree that high secondary mineral formation relative to primary  
254 mineral dissolution drives dissolved  $\delta^7\text{Li}$  high.

255

### 256 *5.1 Comparison of lithium isotopes to river chemistry*

257 It has been demonstrated that Li isotopes are not affected by dissolution  
258 of carbonates, both in the High Himalayas (Kisakürek et al., 2005) and in the  
259 Mackenzie catchments (Millot et al., 2010), but are solely controlled by silicate  
260 weathering. Mixing relationships (e.g. between Ca/Na and Li/Ca) that were used  
261 in those studies to show this are not as apparent in the Ganges, possibly because  
262 secondary processes are affecting both [Ca] (e.g. plant growth/decay) and [Li]  
263 (e.g. secondary mineral destabilisation), as well as effects by the dissolution of  
264 evaporites on Na and possibly Li (Galy and France-Lanord, 1999; Rai et al.,  
265 2010). Nevertheless, it is clear that riverine  $\delta^7\text{Li}$  values are not being controlled  
266 by carbonate weathering, because samples with highest Ca/Na have low  $\delta^7\text{Li}$ ,  
267 while carbonates tend to have isotopically heavy, seawater-like, values (Lechler  
268 et al., 2015; Marriott et al., 2004; Pogge von Strandmann et al., 2013).

269 In a number of river studies, Li/Na ratios have been reported to have  
270 similar behaviour to Li isotope ratios, and the former has been inferred as a  
271 tracer of water-rock interaction time (Dellinger et al., 2015; Liu et al., 2015;  
272 Millot et al., 2010). This is because Na is thought to be significantly more mobile  
273 than Li during weathering, and, generally, little Na is incorporated into  
274 secondary minerals compared to Li. Waters with lowest  $\delta^7\text{Li}$  have highest Li/Na,

275 defining a negative co-variation and thus agreeing with the trend shown in other  
276 studies (Bagard et al., 2015; Dellinger et al., 2015; Liu et al., 2015; Millot et al.,  
277 2010). However, in these Ganges waters, there is significant variation (over an  
278 order of magnitude) in Li/Na for a virtually constant  $\delta^7\text{Li}$  (Fig. 4). This suggests a  
279 degree of decoupling between [Li] and  $\delta^7\text{Li}$  in these waters, which is also  
280 observed in the lack of direct co-variation between these two parameters.  
281 Interestingly, data from the High Himalayas (Kisakürek et al., 2005) exhibit a  
282 similar pattern (Fig. 4), with relatively constant  $\delta^7\text{Li}$  for a high variation in Li/Na  
283 ( $\sim 0.0001$  to  $0.001$ ). Although the data are sparser, the same could be argued for  
284 the Ganges-Brahmaputra study of Bagard et al. (2015).

285 Overall, some of the data from global rivers show a logarithmic  
286 relationship between  $\delta^7\text{Li}$  and Li/Na, apparently consistent with kinetic  
287 fractionation, and possible to simulate with a Rayleigh equation. Given that much  
288 of river weathering is an open system, riverine behaviour should not be able to  
289 be attributed to closed-system Rayleigh behaviour, and we also examine  
290 equilibrium fractionation processes. To assess Rayleigh fractionation factors we  
291 use a standard approach used by a number of studies (Bagard et al., 2015;  
292 Dellinger et al., 2015; Pogge von Strandmann et al., 2012), but in this case we use  
293 an average continental crust  $\delta^7\text{Li}$  of 0‰ as the initial composition, assuming  
294 entirely congruent weathering. There is significant scatter, most likely due to  
295 lithology effects on Li/Na ratios (for example, due to a range of initial Li/Na  
296 compositions or due to the formation of Na-bearing secondary minerals, such as  
297 zeolites (e.g. analcime, chabazite, phillipsite, etc.), or smectites such as Na-  
298 montmorillonite), and similar effects on  $\delta^7\text{Li}$ , because primary lithology will  
299 determine secondary mineralogy, which will affect Li isotope fractionation

300 factors (Millot and Girard, 2007; Pistiner and Henderson, 2003; Pogge von  
301 Strandmann et al., 2010; Pogge von Strandmann et al., 2006; Vigier et al., 2008;  
302 Williams and Hervig, 2005). It is possible that in rivers draining multiple  
303 lithologies, though, less concentrated terrains (such as basaltic ones) do not  
304 contribute enough Li to affect fractionation. For example, the Chambal  
305 tributaries to the Yamuna have similar  $\delta^7\text{Li}$  and [Li] values, despite also draining  
306 basalts (Lupker et al., 2012). However, a best-fit Li isotope Rayleigh fractionation  
307 factor for global data (Fig. 4) is  $\alpha \sim 0.995$  ( $\Delta^7\text{Li} = -5\text{‰}$ ), as also suggested for the  
308 Ganges-Brahmaputra (Bagard et al., 2015). Maximum and minimum  
309 fractionation factors, which incorporate the totality of the data (excluding  
310 Amazonian samples that are controlled by secondary mineral re-dissolution  
311 (Dellinger et al., 2015)) are  $\alpha = 0.985$  ( $\Delta^7\text{Li} = -15\text{‰}$ ) and  $\alpha = 0.9975$  ( $\Delta^7\text{Li} = -$   
312  $2.5\text{‰}$ ). As mentioned above, it is notable that almost all of the High Himalayan  
313 data (Kisakürek et al., 2005) and the Ganges data from this study plot above the  
314 median  $\alpha = 0.995$  line. This study's Ganges samples are encompassed by  
315 fractionation factors of 0.9955 – 0.985, although when precipitation corrected  
316 Li/Na\* ratios are used (using the correction detailed by Frings et al., 2015, using  
317 the methods of other Ganges studies (Bickle et al., 2005; Dalai et al., 2002; Galy  
318 and France-Lanord, 1999; Galy et al., 1999; Rai et al., 2010)), this changes slightly  
319 to 0.995–0.98, with a median fractionation factor of 0.988 ( $\Delta^7\text{Li} = -13\text{‰}$ ). Other  
320 large rivers like the Amazon also plot above the 0.995 line, where their starting  
321 compositions are similar to those of the Ganges (Dellinger et al., 2014).  
322 Generally, sediments from these rivers exhibit a similar range in Li/Na to each  
323 other and to global shales (Fig. 4). In contrast, rivers that drain basaltic terrains  
324 (Iceland, Azores, Columbia River Basalts (Liu et al., 2015; Pogge von Strandmann

325 et al., 2010; Pogge von Strandmann et al., 2006) do have a significantly different  
326 starting Li/Na (Fig. 4), although the effect of using a basaltic starting  $\delta^7\text{Li}$   
327 composition of 3–5‰ higher than the continental crust is relatively minor.

328 Whereas basaltic data follow a Rayleigh relationship (Fig. 4), this study's  
329 Ganges data appear to be closer to an equilibrium (batch) relationship (dashed  
330 lines in Fig. 4), mostly plotting between fractionation factors of 0.97–0.98. Such a  
331 relationship implies that the Ganges reaches a steady-state between primary  
332 rock dissolution and secondary mineral formation (this is discussed in more  
333 detail in Section 5.2), whereas the supply-rich (i.e. kinetically-limited) basaltic  
334 terrains and High Himalayas do not.

335 Generally, then, weathering of large continental crust floodplains such as  
336 that of the Ganges appears to cause an equilibrium-style relationship, requiring  
337 higher Li isotope fractionation factors than basaltic terrains. This is likely due to  
338 the different types of secondary mineral that form in different weathering  
339 environments. For example, kaolinites, which tend to be associated with  
340 weathering of intermediate to felsic continental crust rather than basalt, are  
341 thought to impart relatively high Li isotope fractionation factors (Millot and  
342 Girard, 2007; Pistiner and Henderson, 2003). There therefore appears to be  
343 some degree of lithological control over Li isotope ratios in rivers in general,  
344 because the primary lithology will control secondary mineralogy, and hence the  
345 fractionation factors it imposes (Pogge von Strandmann et al., 2010; Wang et al.,  
346 2015). This means, for example, that the interpretation of Li isotopes as a palaeo-  
347 weathering proxy (Hathorne and James, 2006; Lechler et al., 2015; Misra and  
348 Froelich, 2012; Pogge von Strandmann et al., 2013; Ullmann et al., 2013) requires

349 some knowledge of the weathered lithology to make quantitative interpretations  
350 about the weathering fluxes.

351 Using the median fractionation factors described above for the Ganges,  
352 the same distillation relationships can be used to describe the fraction of Li in  
353 solution, relative to that in the solid phase (Frings et al., 2015; Millot et al., 2010;  
354 Pogge von Strandmann et al., 2012; Vigier et al., 2009). Hence, if the  $\delta^7\text{Li}$  of a  
355 river were 0‰, identical to the source rocks, 100% of Li would be in solution.  
356 For Rayleigh fractionation (median  $\alpha = 0.988$ ), on average 19% of Li is in  
357 solution (2–37% for the full range of  $\alpha$ ), while this number is 20% for  
358 equilibrium fractionation (median  $\alpha = 0.975$ ). Frings et al. (2015) determined  
359 catchment areas and estimated river fluxes to give the yield of major elements.  
360 For Si, they then divided this yield by the fraction of Si in solution, determined  
361 from Si isotope ratios using a Rayleigh relationship, to give the initial Si  
362 mobilisation rate, independent of secondary mineral formation. This determined  
363 that ~75% of Si mobilisation in the Ganges occurs outside the Himalayas, in the  
364 alluvial plain and peninsular rivers.

365 Here, we perform the same type of calculation for Li, which shows that  
366 around 63% of initial Li mobilisation (total ~12 Gmol/yr Li if Rayleigh, ~1.1  
367 Gmol/yr if equilibrium) occurs outside the Himalayas. This percentage is highly  
368 insensitive to the fractionation factor used (the entire range in  $\alpha$  for these  
369 Ganges samples changes this percentage by 0.6%). This therefore shows that  
370 greater silicate weathering occurs away from the mountain areas, which agrees  
371 with estimates based on bulk chemistry (West et al., 2002), and Li isotope  
372 studies from New Zealand (Pogge von Strandmann and Henderson, 2015), as  
373 well as reactive-flow modelling (Bouchez et al., 2013). However, there is a



374 difference in the estimates based on Si isotopes (~25% of initial Si is from the  
375 Himalayas (Frings et al., 2015)), with those based on Li isotopes (~38% of initial  
376 Li is from the Himalayas, where the isotopic analytical uncertainty does not  
377 resolvably affect the final calculations). No analyses are available of Li  
378 concentrations of a broad range of sediments of the Ganges floodplain, and  
379 therefore approximate Ca or Mg fluxes based on Li isotopes cannot be calculated.  
380 The difference between Li and Si isotopes as a tracer is discussed below, but it is  
381 probable that the difference in estimates is due to different mobilities in the  
382 weathering environment. While Li and Si are similarly mobile during basalt  
383 weathering (Pogge von Strandmann et al., 2016), the complex environment of  
384 floodplains such as that of the Ganges, and the general lack of Li concentration  
385 analyses, means that such estimates are not possible yet for these terrains. In  
386 addition, some degree of control by biology over Si isotopes and concentrations  
387 is likely - in particular, due to the intensive agriculture of the Ganges alluvial  
388 plain. In contrast, Li isotopes are unlikely to be directly affected by enhanced  
389 plant growth (Clergue et al., 2015; Lemarchand et al., 2010; Pogge von  
390 Strandmann et al., 2016), and fertilisers in the High Himalayan region are  
391 thought to have higher  $\delta^7\text{Li}$  than any samples observed here (Kisakürek et al.,  
392 2005).

393

#### 394 *5.2 Comparison of lithium isotopes to physical parameters*

395 The samples furthest up the Ganges and its catchment were taken above  
396 the town of Rishikesh, almost 2500 km from the river mouth, and located in the  
397 Himalayan foothills. Lithium concentrations are relatively low here (2–3 ng/ml),  
398 but increase sharply several hundred km downstream (Fig. 2a), apparently when

399 highly concentrated tributaries from the north (with up to ~12 ng/ml Li) merge  
400 with the Ganges. One of the largest tributaries, the Yamuna River, also has  
401 relatively high [Li], and this also appears to serve to keep the Ganges [Li] high.  
402 After the confluence of the Yamuna with the Ganges ~1500 km above the river  
403 mouth, Li concentrations start to decline, and after the Ganges enters the  
404 southern alluvial plain, [Li] is lower than in the Himalayan foothills. This decline  
405 in concentration again appears to be driven by the tributaries in the alluvial  
406 plain, which have low Li concentrations. Enhanced secondary mineral formation  
407 is unlikely to be causing this concentration decline, because Li isotope ratios are  
408 not being changed by whatever process is causing the concentration decrease.  
409 The change in [Li] is more likely a result of dilution by precipitation-sourced  
410 waters, as other elemental concentrations are also affected. However, dissolved  
411 [Li] does not directly co-vary with discharge values, although it must be noted  
412 that these are literature compilations rather than direct snapshot values (Frings  
413 et al., 2015; Jain et al., 2007). There is a co-variation between discharge and [Li]  
414 in the final ~400km, but not before (Fig. 5), suggesting that dilution is not a big  
415 effect on Li concentrations aside from this final part of the Ganges (and that  $\delta^7\text{Li}$   
416 is not affected by this dilution). Such a relationship is opposite to that reported  
417 from the Congo (Henchiri et al., 2016).

418 In contrast, Li isotope ratios exhibit their largest variation in the  
419 headwaters of the Ganges. Including this study, the river at Rishikesh has been  
420 sampled for Li isotopes approximately every decade for the last 30 years (Bagard  
421 et al., 2015; Huh et al., 1998), and has had uniformly low  $\delta^7\text{Li}$  values of ~10–  
422 13‰. In comparison, samples taken 1500–2000 km further downstream by all  
423 three studies are consistently isotopically heavier, with  $\delta^7\text{Li}$  ~20–23‰.

424 Figure 6a summarises all Li isotope studies of rivers associated with the Ganges  
425 as a function of distance from the Main Frontal Thrust (MFT), which delineates  
426 the uplifting areas from the floodplain (Huang et al., 2015). Data from the High  
427 Himalayas (Kisakurek et al., 2005), which eventually drain into the Ganges,  
428 generally have lower  $\delta^7\text{Li}$  than the Ganges mainstream. In these data, rivers with  
429 lower [Li] have higher  $\delta^7\text{Li}$ , so that High Himalayan rivers with high  $\delta^7\text{Li}$  have  
430 little overall influence on the composition of waters downstream. The general  
431 relationship with distance clearly shows that only relatively low  $\delta^7\text{Li}$  values are  
432 from the Himalayan foothills or mountains. Interestingly, the three studies of the  
433 Ganges mainstream were sampled at different time periods, i.e. those of Bagard  
434 et al. (2015) represent a low flow period, while this study represents the end of  
435 peak flooding. Nevertheless, samples from the same location are similar,  
436 implying that hydrological regime does not resolvably affect Li behaviour.

437         After a distance of  $\sim 500$  km of flow,  $\delta^7\text{Li}$  values are relatively constant,  
438 and both the Ganges and its tributaries are close to the global riverine mean of  
439  $\sim 23\text{‰}$  (Huh et al., 1998). Such constant  $\delta^7\text{Li}$  values for such a long distance  
440 imply a balance between mineral dissolution and precipitation, as would be  
441 thought to characterise a floodplain at steady-state, i.e. one that maintains an  
442 approximately constant level of weathering intensity. Our data suggest that the  
443 Ganges floodplain is broadly in steady-state for  $\sim 80\%$  of its flow length, from the  
444 area of Kanpur to the river mouth (Fig. 1 & 2b), and that weathering is only out  
445 of balance in the foothills regions of the studied area.

446         Pogge von Strandmann and Henderson (2015) and Dellinger et al. (2015)  
447 have both showed that Li isotope ratios in rivers tend to be driven lower in  
448 regions of higher uplift and therefore higher denudation and exposure rates,

449 because more fresh primary rock is being made available for dissolution, relative  
450 to the formation of secondary minerals. In contrast, in flatter regions where  
451 uplift and exposure are low (i.e. floodplains), secondary mineral formation  
452 becomes relatively greater, and riverine  $\delta^7\text{Li}$  values increase. These studies are  
453 also backed up by the observation that rivers in the High Himalayas generally  
454 have  $\delta^7\text{Li}$  values lower than the global mean (Huh et al., 1998; Kiskürek et al.,  
455 2005), or indeed lower than values in rivers on the floodplain at the same  
456 distance from the river mouth, as shown by comparing the floodplain-based  
457 Yamuna and the foothills-sourced Ganges Rivers (Fig. 2b).

458         While uplift rates are not available for these samples, in the Himalayan  
459 region, altitude is an approximate facsimile to exposure. Figure 6b shows a  
460 literature compilation of Li isotopes in the Ganges-Brahmaputra catchment area,  
461 and there is a broad co-variation where lower altitude corresponds to higher  
462 dissolved  $\delta^7\text{Li}$ . There is considerable variation in the High Himalayas (Kiskürek  
463 et al., 2005), which may be because very small streams are also represented in  
464 that study, but as described above, rivers with lower  $\delta^7\text{Li}$  will have the greater  
465 influence on riverine signals downstream. Overall, however, it is probable that  
466 the low  $\delta^7\text{Li}$  values observed in the Ganges headwaters are due to relatively  
467 greater primary rock exposure and dissolution (more congruent silicate  
468 weathering), while the increase in  $\delta^7\text{Li}$  further downstream is due to increasing  
469 secondary mineral formation (more incongruent silicate weathering), due to  
470 increased water-rock interaction times (reaction kinetics) driving a greater  
471 degree of secondary mineral oversaturation and precipitation (reaction  
472 thermodynamics).

473

474 *5.3 Li isotopes as a proxy for silicate weathering rates*

475           While Li isotopes are generally thought to be an excellent tracer of silicate  
476 weathering congruency or intensity, a number of studies have also found  
477 correlations between riverine  $\delta^7\text{Li}$  and the silicate weathering rate. In particular,  
478 negative co-variations have been reported from Iceland (Vigier et al., 2009) and  
479 the Mackenzie River basin (Millot et al., 2010) (the Mackenzie River accounts for  
480  $\sim 2\%$  of global riverine discharge (Huh et al., 1998)). Some interpretations of  
481 palaeo  $\delta^7\text{Li}$  data have been based on these two published negative relationships,  
482 and the assumption that clays and the dissolved load co-behave (Dosseto et al.,  
483 2015). Overall, however, it seems highly unlikely that  $\delta^7\text{Li}$  can be used as a  
484 weathering rate tracer, unless the weathering system is extremely simple, and  
485 the secondary mineral formation rate and fractionation factor stays constant,  
486 while the primary mineral dissolution rate is then solely a function of the  
487 weathering rate.

488           In the case of these Ganges data, silicate weathering rates were calculated  
489 from the discharge rates, precipitation-corrected major element data and  
490 catchment areas calculated by Frings et al. (2015), using the methods  
491 demonstrated by numerous other studies, by correcting for silicate and  
492 evaporate components (Dalai et al., 2002; Gaillardet et al., 1999a; Galy and  
493 France-Lanord, 1999; Rai et al., 2010). As shown in Figure 7, there is no  
494 relationship between silicate weathering rate and  $\delta^7\text{Li}$  for these samples ( $r^2 =$   
495 0.01). In other words, for one of the Earth's major rivers, that supplies  $\sim 3\%$  of  
496 the global riverine Li flux (Huh et al., 1998), dissolved Li isotopes are not a tracer  
497 of the silicate weathering rate. Figure 7 also shows data from globally significant

498 rivers responsible for ~30% of the global riverine discharge (Huh et al., 1998),  
499 which similarly exhibit no relationship between  $\delta^7\text{Li}$  and weathering rate.

500 Hence, while some river systems show co-variations between these two  
501 factors, overall it is clear that Li isotopes cannot be used as a weathering rate-  
502 tracer, and therefore modelling must be used to determine any useful  
503 weathering fluxes from riverine or seawater records (Bouchez et al., 2013;  
504 Lechler et al., 2015; Li and West, 2014; Pogge von Strandmann et al., 2013; Pogge  
505 von Strandmann et al., 2014; Vigier and Godderis, 2015; Wanner et al., 2014).

506

#### 507 *5.4 Comparison between Li and Si isotopes*

508 Silicon isotope ratios have also been determined for these samples  
509 (Frings et al., 2015). In theory,  $\delta^{30}\text{Si}$  behaves similarly to  $\delta^7\text{Li}$ , in that both  
510 systems are used as silicate weathering tracers, where secondary minerals  
511 preferentially take up light isotopes, driving river waters and seawater to  
512 isotopically heavy values (De la Rocha et al., 2000; Georg et al., 2006; Georg et al.,  
513 2007; Opfergelt et al., 2013; Opfergelt et al., 2009; Ziegler et al., 2005). In  
514 addition, for Si isotopes, primary productivity (e.g. diatoms) and plant growth  
515 exert an influence, and preferentially take up light isotopes (Opfergelt et al.,  
516 2006). The Ganges's  $\delta^{30}\text{Si}$  values have been interpreted similarly to Li isotopes  
517 by Frings et al. (2015), i.e. controlled by silicate weathering congruency, with  
518 additional, indistinguishable, effects from plants or other biological processes,  
519 and have been used to determine silicate weathering fluxes (Frings et al., 2015).  
520 It therefore makes sense to compare these two tracers, given their behavioural  
521 similarity, but also their differences, as Si is a major structural element of both

522 primary silicate rocks and many secondary minerals, while Li is only a trace  
523 element.

524 Overall, then, there is a positive co-variation between  $\delta^7\text{Li}$  and  $\delta^{30}\text{Si}$  (Fig.  
525 8). This trend is pinned by the Ganges mainstream, which exhibits a good  
526 correlation ( $r^2 = 0.78$ ). Himalayan headwaters are isotopically light (congruent  
527 weathering) for both systems. However, the Ganges tributaries show much  
528 greater relative variability for Si isotopes than for Li isotopes. Thus, while the  
529 Ganges mainstream makes up 80% of the total  $\delta^7\text{Li}$  variation observed, it only  
530 makes up 50% of the  $\delta^{30}\text{Si}$  variability. This difference is likely due to differing  
531 fractionation caused to both systems by secondary minerals, because Si is a  
532 major structural component of many minerals, while Li is a trace element (Pogge  
533 von Strandmann et al., 2012). However, this does not necessarily explain  
534 relatively constant  $\delta^7\text{Li}$  in samples with variable  $\delta^{30}\text{Si}$ , because a given secondary  
535 mineral should impose a set fractionation on both Li and Si isotopes. Differences  
536 in reaction kinetics may therefore be a primary control of the difference in  
537 isotope fractionation. Si may require more time to be incorporated into  
538 neoformed minerals, while Li is at least partially controlled by sorption (Millot  
539 and Girard, 2007; Pistiner and Henderson, 2003; Pogge von Strandmann et al.,  
540 2016; Pogge von Strandmann et al., 2012). Alternatively, Si isotopes are affected  
541 by plant and/or diatom growth, which may be imposing additional, and  
542 potentially quite spatially variable, fractionation (Opfergelt et al., 2006; Opfergelt  
543 et al., 2011), and therefore the  $\delta^{30}\text{Si}$  variability beyond that which correlates with  
544 Li isotopes could be a biologically-induced effect. Hence, the Ganges system, with  
545 its longer water flow time in the alluvial plain compared to most rivers studied  
546 for Li isotopes, would be expected to approach a state where both Li and Si

547 isotopes reach a degree of steady-state. In addition, a co-variation has also been  
548 reported from plant- and organic-poor waters from Iceland (Fig. 8), suggesting  
549 that in systems where biological fractionation of Si isotopes is low, Li and Si  
550 isotopes will behave similarly (Opfergelt et al., 2013), because Li isotopes are  
551 unaffected by plants (Lemarchand et al., 2010; Pogge von Strandmann et al.,  
552 2016).

553

#### 554 *5.5 Global implications of the Ganges Li chemistry*

555 It is clear from the comparison of Li and Si isotopes that silicate  
556 weathering is more congruent (less intense) in the Himalayan foothills of the  
557 Ganges than it is in the alluvial plain. It has equally been shown that on average  
558 High Himalayan catchments are even more congruent (Fontorbe et al., 2013;  
559 Kiskürek et al., 2005). This behaviour makes it abundantly clear that dominant  
560 secondary mineral formation, and hence isotope fractionation, occurs in the  
561 floodplains. This evidence is substantiated by both mineralogical analyses that  
562 suggest that authigenic clays only become dominant in alluvial plains  
563 (Chakrapani et al., 1995), and by other estimates of weathering by solute mass  
564 balance (Galy and France-Lanord, 1999; Lupker et al., 2012; West et al., 2002),  
565 which also suggest that the primary locus of CO<sub>2</sub> drawdown through silicate  
566 weathering is in floodplains rather than steep slopes.

567 Overall, an increase in Himalayan denudation, delivered to the oceans by  
568 the Ganges-Brahmaputra river system, has been argued to be the (or a) cause of  
569 increases in seawater <sup>87</sup>Sr/<sup>86</sup>Sr and <sup>187</sup>Os/<sup>188</sup>Os (Bickle et al., 2005; Galy et al.,  
570 1999; Oliver et al., 2003; Pierson-Wickmann et al., 2002a, b; Sharma et al., 1999).  
571 The increase in Cenozoic seawater δ<sup>7</sup>Li (Hathorne and James, 2006; Misra and



572 Froelich, 2012) has also been interpreted as due to increased Himalayan  
573 weathering (Froelich and Misra, 2014). More recently, data from other uplift and  
574 exposure sites have suggested that mountain regions themselves are only the  
575 drivers of physical erosion, and that the Li isotope fractionation occurs in the  
576 floodplains (Dellinger et al., 2015; Pogge von Strandmann and Henderson, 2015).

577         Interestingly, the Ganges controls the Li flux to the oceans to a similar  
578 extent as it does the Sr or Os fluxes, despite the latter two systems also having  
579 carbonate sources. The Ganges provides ~3% of the total riverine supply of Li to  
580 the oceans (compared to 2% of Os (Levasseur et al., 1999) and ~3% of Sr  
581 (Krishnaswami et al., 1992)), and the whole Ganges-Brahmaputra system ~7%  
582 (Huh et al., 1998), with another estimated 2% of the total flux provided by  
583 groundwater flow into the Bengal Basin (Bagard et al., 2015). Combined, the  
584 three main mountain-sourced river systems with floodplains that greatly  
585 increased in size during the Cenozoic (Ganges-Brahmaputra, Amazon and  
586 Orinoco) provide almost 16% of the modern global Li flux from rivers to the  
587 oceans, compared to an estimated ~20% for Sr (Raymo et al., 1988). The three  
588 rivers mentioned above would have to increase their mean  $\delta^7\text{Li}$  by 30–40‰ to  
589 drive the observed seawater change at equilibrium, with no change in flux, which  
590 is extremely unlikely, given observations of modern rivers. Even the evolution of  
591 their floodplains (Pogge von Strandmann and Henderson, 2015) is unlikely to be  
592 responsible for the entire change in seawater  $\delta^7\text{Li}$ . Hence, the relationship  
593 between continental weathering changes and seawater  $\delta^7\text{Li}$  is not  
594 straightforward, and other Cenozoic changes, such as a “sink-shift” (Li and West,  
595 2014) or temperature-dependent changes in deep-ocean fractionation factors

596 (Coogan and Dosso, 2015), may have to be invoked in combination with a  
597 weathering change.

598         The other inference that can be made from these Ganges data for the  
599 Cenozoic evolution of seawater  $\delta^7\text{Li}$  is that it appears that growth of the Ganges  
600 floodplain beyond  $\sim 500\text{km}$  from the Himalayan foothills would no longer change  
601 seawater  $\delta^7\text{Li}$ , as evidenced by the near constant riverine  $\delta^7\text{Li}$  values. Beyond  
602 this point, under present climatic conditions, the floodplain is in approximate  
603 steady-state for Li isotopes (and also for Si isotopes (Frings et al., 2015)). A  
604 similar observation can be made for the Amazon, where most fractionation  
605 occurs close to the foothills, and then remains constant across the floodplain  
606 (Dellinger et al., 2015). If present-day measurements can be used as an analogy  
607 for general Cenozoic behaviour (as used for Sr isotopes (Galy et al., 1999)), then  
608 the final 2000 km of Ganges flow creates no change in  $\delta^7\text{Li}$ , and the evolution of  
609 the floodplain beyond  $\sim 500\text{km}$  will not create further change in seawater  $\delta^7\text{Li}$   
610 once this has reached equilibrium with regards to input.

611

## 612 6.0 Conclusions

613         This study has analysed Li isotopes from over 50 samples of the Ganges  
614 river and its tributaries, representing over an order of magnitude increase in  
615 sampling density compared to previous studies. Lithium isotope ratios are fairly  
616 constant for the lower  $\sim 2000\text{ km}$  of flow of the Ganges, and  $\delta^7\text{Li}$  only decreases  
617 at the head of the river in the Himalayan foothills. Silicate weathering is  
618 therefore at its most congruent in mountainous regions where uplift and fresh  
619 silicate exposure rates are high. These data were used to calculate a Li yield from  
620 primary rock, indicating that over 63% of Ganges Li stems from the floodplains,

621 rather than the mountainous regions. This observation agrees with those made  
622 from bulk river chemistry, as well as Si isotopes, although the precise fraction of  
623 Li and Si coming from the Himalayas appears to be different, based on their  
624 individual isotope systems, likely due to a combination of secondary mineral  
625 reaction kinetics, and the influence of biology over Si.

626 Overall, despite some publications using Li isotopes as a tracer for the  
627 silicate weathering rate, there is no correlation whatsoever between Ganges  $\delta^7\text{Li}$   
628 and silicate weathering rates. The lack of such a correlation in one of the Earth's  
629 major rivers strongly indicates that  $\delta^7\text{Li}$  also cannot be used as a direct palaeo-  
630 weathering rate tracer.

631 Finally, the Li isotope data (which are controlled by the ratio of primary  
632 mineral dissolution relative to secondary mineral formation) suggest that the  
633 Ganges floodplains are broadly at steady-state, with dissolution and transport in  
634 equilibrium. The close-to-constant  $\delta^7\text{Li}$  values for the final 2000km of Ganges  
635 flow also suggest that once the size of the alluvial plain reached more than ~500  
636 km under present climatic conditions, the Ganges exerted little influence on the  
637 changing Cenozoic seawater  $\delta^7\text{Li}$ .

638

639

#### 640 Acknowledgements

641 Analyses were supported by PPvS's NERC Advanced Research Fellowship  
642 NE/I020571/2. We thank Wim Clymans for help with fieldwork, Chakrapani  
643 Govind for logistical support and Will Gray for assistance with ICP-OES/MS  
644 analysis. We thank Paul Tomascak, Maarten Lupker and an anonymous reviewer  
645 for their insightful comments.

646

647

648 Bagard, M.-L., West, A.J., Newman, K. and Basu, A.K. (2015) Lithium isotope  
649 fractionation in the Ganges–Brahmaputra floodplain and implications for  
650 groundwater impact on seawater isotopic composition. *Earth Planet. Sci. Lett.*  
651 432, 404–414,  
652 Berner, R.A. (2003) The long-term carbon cycle, fossil fuels and atmospheric  
653 composition. *Nature* 426, 323–326,  
654 Berner, R.A., Lasaga, A.C. and Garrels, R.M. (1983) The Carbonate-Silicate  
655 Geochemical Cycle and Its Effect on Atmospheric Carbon-Dioxide over the Past  
656 100 Million Years. *Am. J. Sci.* 283, 641–683,  
657 Bickle, M.J., Chapman, H.J., Bunbury, J., Harris, N.B.W., Fairchild, I.J., Ahman, T. and  
658 Pomies, C. (2005) Relative contributions of silicate and carbonate rocks to  
659 riverine Sr fluxes in the headwaters of the Ganges. *Geochim. Cosmochim. Acta* 69,  
660 2221–2240,  
661 Bouchez, J., von Blanckenburg, F. and Schuessler, J.A. (2013) Modeling novel  
662 stable isotope ratios in the weathering zone. *Am. J. Sci.* 313,  
663 10.2475/04.2013.001.  
664 Chakrapani, G.J., Subramanian, V., Gibbs, R.J. and Jha, P.K. (1995) Size  
665 characteristics and mineralogy of suspended sediments of the Ganges river,  
666 India. 25, 192–196,  
667 Clergue, C., Dellinger, M., Buss, H.L., Gaillardet, J., Benedetti, M.F. and Dessert, C.  
668 (2015) Influence of atmospheric deposits and secondary minerals on Li isotopes  
669 budget in a highly weathered catchment, Guadeloupe (Lesser Antilles). *Chem.*  
670 *Geol.* 414, 28–41,  
671 Coogan, L.A. and Dosso, S.E. (2015) Alteration of ocean crust provides a strong  
672 temperature dependent feedback on the geological carbon cycle and is a primary  
673 driver of the Sr-isotopic composition of seawater. *Earth Planet. Sci. Lett.* 415, 38–  
674 46,  
675 Dalai, T.K., Krishnaswami, S. and Sarin, M.M. (2002) Major ion chemistry in the  
676 headwaters of the Yamuna river system: Chemical weathering, its temperature  
677 dependence and CO<sub>2</sub> consumption in the Himalaya. *Geochim. Cosmochim. Acta*  
678 66, 3397–3416,  
679 De la Rocha, C.L., Brzezinski, M.A. and DeNiro, M.J. (2000) A first look at the  
680 distribution of the stable isotopes of silicon in natural waters. *Geochim.*  
681 *Cosmochim. Acta* 64, 2467–2477,  
682 Dellinger, M., Gaillardet, J., Bouchez, J., Calmels, D., Galy, V., Hilton, R.G., Louvat, P.  
683 and France-Lanord, C. (2014) Lithium isotopes in large rivers reveal the  
684 cannibalistic nature of modern continental weathering and erosion. *Earth Planet.*  
685 *Sci. Lett.* 401, 359–372,  
686 Dellinger, M., Gaillardet, J., Bouchez, J., Calmels, D., Louvat, P., Dosseto, A., Gorge,  
687 C., Alanoca, L. and Maurice, L. (2015) Riverine Li isotope fractionation in the  
688 Amazon River basin controlled by the weathering regimes. *Geochim. Cosmochim.*  
689 *Acta* 164, 71–93,  
690 Dosseto, A., Vigier, N., Joassnes-Boyau, R., Moffat, I., Singh, T. and Srivastava, P.  
691 (2015) Rapid response of silicate weathering rates to climate change in the  
692 Himalaya. *Geochemical Perspectives Letters* 1, 10–19,

693 Elliott, T., Thomas, A., Jeffcoate, A. and Niu, Y.L. (2006) Lithium isotope evidence  
694 for subduction-enriched mantle in the source of mid-ocean-ridge basalts. *Nature*  
695 443, 565–568,

696 Flesch, G.D., Anderson, A.R. and Svec, H.J. (1973) A secondary isotopic standard  
697 for  $6\text{Li}/7\text{Li}$  determinations. *Int. J. Mass Spectrom. Ion Process.* 12, 265–272,

698 Fontorbe, G., De la Rocha, C.L., Chapman, H.J. and Bickle, M.J. (2013) The silicon  
699 isotopic composition of the Ganges and its tributaries. *Earth Planet. Sci. Lett.* 381,  
700 21–30,

701 Frings, P.J., Clymans, W., Fontorbe, G., Gray, W., Chakrapani, G.J., Conley, D.J. and  
702 De la Rocha, C.L. (2015) Silicate weathering in the Ganges alluvial plain. *Earth*  
703 *Planet. Sci. Lett.* 427, 136–148,

704 Froelich, P.N. and Misra, S. (2014) Was the late Paleocene-early Eocene hot  
705 because Earth was flat? An ocean lithium isotope view of mountain building,  
706 continental weathering, carbon dioxide, and Earth's Cenozoic climate.  
707 *Oceanography* 27, 36–49,

708 Gaillardet, J., Dupré, B. and Allègre, C.J. (1999a) Geochemistry of large river  
709 suspended sediments: silicate weathering or recycling tracer? *Geochim.*  
710 *Cosmochim. Acta* 63, 4037–4051,

711 Gaillardet, J., Dupre, B., Louvat, P. and Allegre, C.J. (1999b) Global silicate  
712 weathering and  $\text{CO}_2$  consumption rates deduced from the chemistry of large  
713 rivers. *Chem. Geol.* 159, 3–30,

714 Galy, A. and France-Lanord, C. (1999) Weathering processes in the Ganges–  
715 Brahmaputra basin and the riverine alkalinity budget. *Chem. Geol.* 159, 31–60,

716 Galy, A., France-Lanord, C. and Derry, L.A. (1999) The strontium isotopic budget  
717 of Himalayan Rivers in Nepal and Bangladesh. *Geochim. Cosmochim. Acta* 63,  
718 1905–1925,

719 Georg, R.B., Reynolds, B.C., Frank, M. and Halliday, A.N. (2006) Mechanisms  
720 controlling the silicon isotopic compositions of river waters. *Earth Planet. Sci.*  
721 *Lett.* 249, 290–306, 10.1016/j.epsl.2006.07.006I.

722 Georg, R.B., Reynolds, B.C., West, A.J., Burton, K.W. and Halliday, A.N. (2007)  
723 Silicon isotope variations accompanying basalt weathering in Iceland. *Earth*  
724 *Planet. Sci. Lett.* 261, 476–490,

725 Georg, R.B., West, A.J., Basu, A.R. and Halliday, A.N. (2009) Silicon fluxes and  
726 isotope composition of direct groundwater discharge into the Bay of Bengal and  
727 the effect on the global ocean silicon isotope budget. *Earth Planet. Sci. Lett.* 283,  
728 67–74,

729 Gíslason, S.R., Oelkers, E. and Snorrason, A. (2006) Role of river-suspended  
730 material in the global carbon cycle. *Geology* 34, 49–52,

731 Gíslason, S.R., Oelkers, E.H., Eiriksdóttir, E.S., Kardjilov, M.I., Gísladóttir, G.,  
732 Sigfusson, B., Snorrason, A., Elefsen, S., Hardardóttir, J., Torssander, P. and  
733 Oskarsson, N. (2009) Direct evidence of the feedback between climate and  
734 weathering. *Earth Planet. Sci. Lett.* 277, 213–222, 10.1016/j.epsl.2008.10.018I.

735 Hathorne, E.C. and James, R.H. (2006) Temporal record of lithium in seawater: a  
736 tracer for silicate weathering? *Earth Planet. Sci. Lett.* 246, 393–406,

737 Henchiri, S., Gaillardet, J., Dellinger, M., Bouchez, J. and Spencer, R.G.M. (2016)  
738 Riverine dissolved lithium isotopic signatures in low-relief central Africa and  
739 their link to weathering regimes. *Geophysical Research Letters* 43, 10.1002/  
740 2016GL067711.I.

741 Huang, W., van Hinsbergen, D.J.J. and Kapp, P. (2015) Paleolatitudes of the  
742 Tibetan Himalaya from primary and secondary magnetizations of Jurassic to  
743 Lower Cretaceous sedimentary rocks. *Geochem. Geophys. Geosyst.*,  
744 10.1002/2014GC005624I.

745 Huh, Y., Chan, L.H. and Edmond, J.M. (2001) Lithium isotopes as a probe of  
746 weathering processes: Orinoco River. *Earth Planet. Sci. Lett.* 194, 189–199,

747 Huh, Y., Chan, L.H., Zhang, L. and Edmond, J.M. (1998) Lithium and its isotopes in  
748 major world rivers: Implications for weathering and the oceanic budget.  
749 *Geochim. Cosmochim. Acta* 62, 2039–2051,

750 Jain, S.K., Agarwal, P.K. and Singh, V.P. (2007) *Hydrology and Water Resources of*  
751 *India*. Springer.

752 Jeffcoate, A.B., Elliott, T., Thomas, A. and Bouman, C. (2004) Precise, small sample  
753 size determinations of lithium isotopic compositions of geological reference  
754 materials and modern seawater by MC-ICP-MS. *Geostandards and Geoanalytical*  
755 *Research* 28, 161-172,

756 Kisakürek, B., James, R.H. and Harris, N.B.W. (2005) Li and  $\delta^7\text{Li}$  in Himalayan  
757 rivers: Proxies for silicate weathering? *Earth Planet. Sci. Lett.* 237, 387–401,

758 Krishnaswami, S., Trivedi, J.R., Sarin, M.M., Ramesh, R. and Sharma, K.K. (1992)  
759 Strontium isotopes and rubidium in the Ganga-Brahmaputra river system:  
760 Weathering in the Himalaya, fluxes to the Bay of Bengal and contributions to the  
761 evolution of oceanic  $87\text{Sr}/86\text{Sr}$ . *Earth Planet. Sci. Lett.* 109, 243–253,

762 Lechler, M., Pogge von Strandmann, P.A.E., Jenkyns, H.C., Prosser, G. and Parente,  
763 M. (2015) Lithium-isotope evidence for enhanced silicate weathering during OAE  
764 1a (Early Aptian Selli event). *Earth Planet. Sci. Lett.* 432, 210–222,

765 Lemarchand, E., Chabaux, F., Vigier, N., Millot, R. and Pierret, M.C. (2010) Lithium  
766 isotope systematics in a forested granitic catchment (Strengbach, Vosges  
767 Mountains, France). *Geochim. Cosmochim. Acta* 74, 4612-4628,

768 Levasseur, S., Birck, J.L. and Allègre, C.J. (1999) The osmium riverine flux and the  
769 oceanic mass balance of osmium. *Earth Planet. Sci. Lett.* 174, 7–23,

770 Li, G. and West, A.J. (2014) Evolution of Cenozoic seawater lithium isotopes:  
771 Coupling of global denudation regime and shifting seawater sinks. *Earth Planet.*  
772 *Sci. Lett.* 401, 284–293,

773 Liu, X.-M., Wanner, C., Rudnick, R.L. and McDonough, W.F. (2015) Processes  
774 controlling  $\delta^7\text{Li}$  in rivers illuminated by study of streams and groundwaters  
775 draining basalts. *Earth Planet. Sci. Lett.* 409, 212–224,

776 Lupker, M., France-Lanord, C., Galy, V., Lave, J., Gaillardet, J., Gajurel, A.P.,  
777 Guilmette, C., Rahman, M., Singh, S.K. and Sinha, R. (2012) Predominant  
778 floodplain over mountain weathering of Himalayan sediments (Ganga basin).  
779 *Geochim. Cosmochim. Acta* 84, 410–432,

780 Maher, K. and Chamberlain, C.P. (2014) Hydrologic Regulation of Chemical  
781 Weathering and the Geologic Carbon Cycle. *Science* 343, 1502–1504,

782 Marriott, C.S., Henderson, G.M., Crompton, R., Staubwasser, M. and Shaw, S.  
783 (2004) Effect of mineralogy, salinity, and temperature on Li/Ca and Li isotope  
784 composition of calcium carbonate. *Chem. Geol.* 212, 5–15,

785 McArthur, J.M., Howarth, R.J. and Bailey, T.R. (2001) Strontium isotope  
786 stratigraphy: LOWESS version 3: Best fit to the marine Sr-isotope curve for 0-509  
787 Ma and accompanying look-up table for deriving numerical age. *Journal of*  
788 *Geology* 109, 155-170,

789 Millot, R. and Girard, J.P. (2007) Lithium Isotope Fractionation during adsorption  
790 onto mineral surfaces, Int. meet., Clays in natural & engineered barriers for  
791 radioactive waste confinement, Lille, France.

792 Millot, R., Vigier, N. and Gaillardet, J. (2010) Behaviour of lithium and its isotopes  
793 during weathering in the Mackenzie Basin, Canada. *Geochim. Cosmochim. Acta*  
794 74, 3897–3912,

795 Misra, S. and Froelich, P.N. (2012) Lithium Isotope History of Cenozoic Seawater:  
796 Changes in Silicate Weathering and Reverse Weathering. *Science* 335, 818–823,  
797 Oelkers, E.H., Jones, M.T., Pearce, C.R., Jeandel, C., Eiriksdottir, E.S. and Gislason,  
798 S.R. (2012) Riverine particulate material dissolution in seawater and its  
799 implications for the global cycles of the elements. *C. R. Geosci.* 344, 646–651,  
800 Oliver, L., Harris, N., Bickle, M., Chapman, H., Dise, N. and Horstwood, M. (2003)  
801 Silicate weathering rates decoupled from the  $^{87}\text{Sr}/^{86}\text{Sr}$  ratio of the dissolved load  
802 during Himalayan erosion. *Chem. Geol.* 201, 119–139,  
803 Opfergelt, S., Burton, K.W., Pogge von Strandmann, P.A.E., Gislason, S.R. and  
804 Halliday, A.N. (2013) Riverine silicon isotope variations in glaciated basaltic  
805 terrains: Implications for the Si delivery to the ocean over glacial–interglacial  
806 intervals. *Earth Planet. Sci. Lett.* 369–370, 211–219,  
807 Opfergelt, S., Cardinal, D., Henriot, C., Drave, X., Andre, L. and Delvaux, B. (2006)  
808 Silicon Isotopic Fractionation by Banana (*Musa* spp.) Grown in a Continuous  
809 Nutrient Flow Device. *Plant Soil* 285, 333–345,  
810 Opfergelt, S., de Bournonville, G., Cardinal, D., Andre, L., Delstanche, S. and  
811 Delvaux, B. (2009) Impact of soil weathering degree on silicon isotopic  
812 fractionation during adsorption onto iron oxides in basaltic ash soils, Cameroon.  
813 *Geochim. Cosmochim. Acta* 73, 7226–7240,  
814 Opfergelt, S., Eiriksdottir, E.S., Burton, K.W., Einarsson, A., Siebert, C., Gislason,  
815 S.R. and Halliday, A.N. (2011) Quantifying the impact of freshwater diatom  
816 productivity on silicon isotopes and silicon fluxes: Lake Myvatn, Iceland. *Earth*  
817 *Planet. Sci. Lett.* 305, 73–82, 10.1016/j.epsl.2011.02.043I.

818 Palmer, M.R. and Edmond, J.M. (1992) Controls over the strontium isotope  
819 composition of river water. *Geochim. Cosmochim. Acta* 56, 2099–2111,  
820 Peucker-Ehrenbrink, B. and Ravizza, G. (2000) The marine osmium isotope  
821 record. *Terra Nova* 12, 205–219,  
822 Peucker-Ehrenbrink, B., Ravizza, G. and Hofmann, A.W. (1995) The Marine Os-  
823 187/Os-186 Record of the Past 80-Million Years. *Earth Planet. Sci. Lett.* 130, 155-  
824 167,  
825 Phan, T.T., Capo, R.C., Stewart, B.W., Macpherson, G.L., Rowan, E.L. and Hammack,  
826 R.W. (2016) Factors controlling Li concentration and isotopic composition in  
827 formation waters and host rocks of Marcellus Shale, Appalachian Basin. *Chem.*  
828 *Geol.* 420, 162–179,  
829 Pierson-Wickmann, A.C., Reisberg, L. and France-Lanord, C. (2002a) Behavior of  
830 Re and Os during low-temperature alteration: Results from Himalayan soils and  
831 altered black shales. *Geochim. Cosmochim. Acta* 66, 1539–1548,  
832 Pierson-Wickmann, A.C., Reisberg, L. and France-Lanord, C. (2002b) Impure  
833 marbles of the Lesser Himalaya: another source of continental radiogenic  
834 osmium. *Earth Planet. Sci. Lett.* 204, 203–214,  
835 Pistiner, J.S. and Henderson, G.M. (2003) Lithium-isotope fractionation during  
836 continental weathering processes. *Earth Planet. Sci. Lett.* 214, 327–339,

837 Pogge von Strandmann, P.A.E., Burton, K.W., James, R.H., van Calsteren, P. and  
838 Gislason, S.R. (2010) Assessing the role of climate on uranium and lithium  
839 isotope behaviour in rivers draining a basaltic terrain. *Chem. Geol.* 270, 227–239,  
840 Pogge von Strandmann, P.A.E., Burton, K.W., James, R.H., van Calsteren, P.,  
841 Gislason, S.R. and Mokadem, F. (2006) Riverine behaviour of uranium and  
842 lithium isotopes in an actively glaciated basaltic terrain. *Earth Planet. Sci. Lett.*  
843 251, 134–147,  
844 Pogge von Strandmann, P.A.E., Burton, K.W., Opfergelt, S., Eiriksdottir, E.S.,  
845 Murphy, M.J., Einarsson, A. and Gislason, S.R. (2016) The effect of hydrothermal  
846 spring weathering processes and primary productivity on lithium isotopes: Lake  
847 Myvatn, Iceland. *Chem. Geol.* in press, 10.1016/j.chemgeo.2016.02.0261.  
848 Pogge von Strandmann, P.A.E., Elliott, T., Marschall, H.R., Coath, C., Lai, Y.J.,  
849 Jeffcoate, A.B. and Ionov, D.A. (2011) Variations of Li and Mg isotope ratios in  
850 bulk chondrites and mantle xenoliths. *Geochim. Cosmochim. Acta* 75, 5247–  
851 5268,  
852 Pogge von Strandmann, P.A.E. and Henderson, G.M. (2015) The Li isotope  
853 response to mountain uplift. *Geology* 43, 67–70,  
854 Pogge von Strandmann, P.A.E., Jenkyns, H.C. and Woodfine, R.G. (2013) Lithium  
855 isotope evidence for enhanced weathering during Oceanic Anoxic Event 2.  
856 *Nature Geoscience* 6, 668–672,  
857 Pogge von Strandmann, P.A.E., Opfergelt, S., Lai, Y.J., Sigfusson, B., Gislason, S.R.  
858 and Burton, K.W. (2012) Lithium, magnesium and silicon isotope behaviour  
859 accompanying weathering in a basaltic soil and pore water profile in Iceland.  
860 *Earth Planet. Sci. Lett.* 339–340, 11–23,  
861 Pogge von Strandmann, P.A.E., Porcelli, D., James, R.H., van Calsteren, P., Schaefer,  
862 B.F., Cartwright, I., Reynolds, B.C. and Burton, K.W. (2014) Chemical weathering  
863 processes in the Great Artesian Basin: Evidence from lithium and silicon  
864 isotopes. *Earth Planet. Sci. Lett.* 406, 24–36,  
865 Rad, S., Rive, K., Vittecoq, B., Cerdan, O. and Allegre, C.J. (2013) Chemical  
866 weathering and erosion rates in the Lesser Antilles: An overview in Guadeloupe,  
867 Martinique and Dominica. *Journal of South American Earth Sciences* 45, 331–344,  
868 10.1016/j.jsames.2013.03.004I.  
869 Rai, S.K., Singh, S.K. and Krishnaswami, S. (2010) Chemical weathering in the  
870 plain and peninsular sub-basins of the Ganga: Impact on major ion chemistry and  
871 elemental fluxes. *Geochim. Cosmochim. Acta* 74, 2340–2355,  
872 Raymo, M.E. (1994) The Himalayas, organic carbon burial, and climate in the  
873 Miocene. *Paleoceanography* 9, 399–404,  
874 Raymo, M.E. and Ruddiman, W.F. (1992) Tectonic Forcing of Late Cenozoic  
875 Climate. *Nature* 359, 117–122,  
876 Raymo, M.E., Ruddiman, W.F. and Froelich, P.N. (1988) Influence of late Cenozoic  
877 mountain building on ocean geochemical cycles *Geology* 16, 649–653,  
878 Sauzeat, L., Rudnick, R.L., Chauvel, C., Garçon, M. and Tang, M. (2015) New  
879 perspectives on the Li isotopic composition of the upper continental crust and its  
880 weathering signature. *Earth Planet. Sci. Lett.* 428, 181–192,  
881 Savage, P.S., Georg, R.B., Armytage, R.M.G., Williams, H.M. and Halliday, A.N.  
882 (2010) Silicon isotope homogeneity in the mantle. *Earth Planet. Sci. Lett.* 295,  
883 139–146,



884 Sharma, M., Wasserburg, G.J., Hoffmann, A.W. and Chakrapani, G.J. (1999)  
885 Himalayan uplift and osmium isotopes in oceans and rivers. *Geochim.*  
886 *Cosmochim. Acta* 63, 4005-4012,  
887 Teng, F.Z., McDonough, W.F., Rudnick, R.L., Dalpe, C., Tomascak, P.B., Chappell,  
888 B.W. and Gao, S. (2004) Lithium isotopic composition and concentration of the  
889 upper continental crust. *Geochim. Cosmochim. Acta* 68, 4167–4178,  
890 Tomascak, P.B., Langmuir, C.H., Le Roux, P.J. and Shirey, S.B. (2008) Lithium  
891 isotopes in global mid-ocean ridge basalts. *Geochim. Cosmochim. Acta*, 1626-  
892 1637,  
893 Torres, M.A., West, A.J. and Li, G. (2014) Sulphide oxidation and carbonate  
894 dissolution as a source of CO<sub>2</sub> over geological timescales. *Nature* 507, 346–349,  
895 Ullmann, C.V., Campbell, H.J., Frei, R., Hesselbo, S.P., Pogge von Strandmann,  
896 P.A.E. and Korte, C. (2013) Partial diagenetic overprint of Late Jurassic  
897 belemnites from New Zealand: Implications for the preservation potential of  
898  $\delta^7\text{Li}$  values in calcite fossils. *Geochim. Cosmochim. Acta* 120, 80–96,  
899 Vigier, N., Decarreau, A., Millot, R., Carignan, J., Petit, S. and France-Lanord, C.  
900 (2008) Quantifying Li isotope fractionation during smectite formation and  
901 implications for the Li cycle. *Geochim. Cosmochim. Acta* 72, 780–792,  
902 Vigier, N., Gislason, S.R., Burton, K.W., Millot, R. and Mokadem, F. (2009) The  
903 relationship between riverine lithium isotope composition and silicate  
904 weathering rates in Iceland. *Earth Planet. Sci. Lett.* 287, 434–441,  
905 Vigier, N. and Godderis, Y. (2015) A new approach for modeling Cenozoic oceanic  
906 lithium isotope paleo-variations: the key role of climate. *Climate of the Past* 11,  
907 635–645,  
908 Walker, J.C.G., Hays, P.B. and Kasting, J.F. (1981) A Negative Feedback Mechanism  
909 for the Long-Term Stabilization of Earths Surface-Temperature. *Journal of*  
910 *Geophysical Research-Oceans and Atmospheres* 86, 9776-9782,  
911 Wang, Q.-L., Chetelat, B., Zhao, Z.-Q., Ding, H., Li, S.-L., Wang, B.-L., Li, J. and Liu, X.-  
912 L. (2015) Behavior of lithium isotopes in the Changjiang River system: Sources  
913 effects and response to weathering and erosion. *Geochim. Cosmochim. Acta* 151,  
914 117–132,  
915 Wanner, C., Sonnenthal, E.L. and Liu, X.-M. (2014) Seawater  $\delta^7\text{Li}$ : A direct proxy  
916 for global CO<sub>2</sub> consumption by continental silicate weathering? *Chem. Geol.* 381,  
917 154–167,  
918 West, A.J. (2012) Thickness of the chemical weathering zone and implications for  
919 erosional and climatic drivers of weathering and for carbon-cycle feedbacks.  
920 *Geology*, 10.1130/G33041.1I.  
921 West, A.J., Bickle, M.J., Collins, R. and Brasington, J. (2002) Small-catchment  
922 perspective on Himalayan weathering fluxes. *Geology* 30, 355–358,  
923 West, A.J., Galy, A. and Bickle, M. (2005) Tectonic and climatic controls on silicate  
924 weathering. *Earth Planet. Sci. Lett.* 235, 211–228,  
925 Williams, L.B. and Hervig, R.L. (2005) Lithium and boron isotopes in illite-  
926 smectite: The importance of crystal size. *Geochim. Cosmochim. Acta* 69, 5705-  
927 5716,  
928 Wimpenny, J., Gislason, S.R., James, R.H., Gannoun, A., Pogge von Strandmann,  
929 P.A.E. and Burton, K.W. (2010a) The behaviour of Li and Mg isotopes during  
930 primary phase dissolution and secondary mineral formation in basalt. *Geochim.*  
931 *Cosmochim. Acta* 74, 5259-5279,

932 Wimpenny, J., James, R.H., Burton, K.W., Gannoun, A., Mokadem, F. and Gislason,  
933 S.R. (2010b) Glacial effects on weathering processes: New insights from the  
934 elemental and lithium isotopic composition of West Greenland rivers Earth  
935 Planet. Sci. Lett. 290, 427-437,  
936 Witherow, R.A., Berry Lyons, W. and Henderson, G.M. (2010) Lithium isotopic  
937 composition of the McMurdo Dry Valleys aquatic systems. Chem. Geol. 275, 139-  
938 147,  
939 Wunder, B., Meixner, A., Romer, R.L. and Heinrich, W. (2006) Temperature-  
940 dependent isotopic fractionation of lithium between clinopyroxene and high-  
941 pressure hydrous fluids. Contrib. Mineral. Petrol. 151, 112-120,  
942 Ziegler, K., Chadwick, O.A., Brzezinski, M.A. and Kelly, E.F. (2005) Natural  
943 variations of delta Si-30 ratios during progressive basalt weathering, Hawaiian  
944 Islands. Geochim. Cosmochim. Acta 69, 4597-4610,  
945  
946  
947  
948  
949  
950  
951

Sample	River	Degrees North	Degrees East	Altitude (m)	Li (ng/ml)	$\delta^7\text{Li}$	2sd	Sil w.r. (t/km <sup>2</sup> /yr)
1	Bhagirathi	30.156	78.603	648	3.23	10.9	0.9	
2	Alaknanda	30.145	78.601	476	2.29	10.7	0.5	
4	Ganga	30.127	78.354	353	3.03	12.9	0.1	8.37
5	Yamuna	28.748	77.226	210	6.65	22.0	0.4	10.3
6	Ganga	28.827	78.154	205	7.10	17.5	0.3	
7	Ramganga	28.666	78.896	185	6.03	23.0	1.0	
8	Unnamed Trib to Ganga	28.031	78.780	170	11.7	23.5	0.8	
9	Ganga	27.930	78.858	165	7.03	16.4	0.2	
10	Yamuna	27.177	78.043	157	10.8	18.4	0.1	
11	Unnamed Trib to Yamuna	26.963	78.365	142	7.60	21.6	0.5	
12	Chambal	26.870	78.367	138	6.72	18.9	0.2	
13	Yamuna	26.602	79.119	113	9.51	19.9	0.2	
14	Chambal Unknown Trib to	26.549	79.088	125	6.50	19.3	0.8	4.89
15	Chambal	26.435	79.209	105	9.29	20.3	0.1	
16	Yamuna	26.425	79.246	105	7.63	22.0	0.2	
17	Ganga	27.010	79.987	127	6.45	21.9	0.1	
18	Unnamed Trib to Ganga	27.271	79.949	133	6.58	16.8	0.3	
19	Ramganga	27.498	79.696	137	6.13	24.8	0.6	19.1
20	Ganga	27.399	79.628	138	6.95	20.6	0.1	

21	Ganga	26.438	80.412	116	5.95	19.4	0.7	
22	Yamuna	25.955	80.160	110	7.59	22.1	0.7	
23	Betwa	25.944	80.156	107	5.52	20.8	0.1	5.09
24	Unnamed Trib to Yamuna	25.654	80.148	111	7.60	19.4	0.9	
25	Ken	25.480	80.313	96	4.61	22.5	0.2	6.39
26	Yamuna (South)	25.708	80.604	87	6.55	21.0	0.8	
27	Yamuna (North Bank)	25.714	80.607	87	6.68	21.5	0.6	
28	Yamuna	25.425	81.882	87	6.14	21.3	0.1	6.87
29	Ganga	25.427	81.887	86	6.39	19.1	0.5	
30	Tons	25.243	82.041	72	5.20	20.3	0.5	3.56
31	Ganga	25.309	82.076	89	6.35	20.9	0.6	
33	Ganga	25.152	82.546	64	5.60	20.2	0.2	
34	Varuna	25.341	82.981	71	6.41	20.0	0.2	
35	Ganga	25.290	83.006	82	6.53	21.2	0.1	
36	Gomati	25.506	83.142	66	6.32	21.4	0.3	5.84
37	Ganga	25.501	83.168	75	6.72	20.9	0.5	
38	Ganga	25.535	83.215	61	2.96	20.6	0.3	
39	Ganga	25.679	84.719	60	6.25	21.2	0.3	
40	Son	25.564	84.790	65	0.43	21.9	0.5	5.17
41	Ghaghara	25.821	84.590	61	6.01	20.9	0.8	6.63
42	Ganga	25.730	84.829	62	2.39	20.7	0.5	
43	Gandak	25.702	85.198	57	3.42	16.7	0.4	9.85
44	Ganga	25.615	85.201	52	2.00	21.7	1.0	
45	Ganga	25.381	86.001	49	2.32	20.8	0.6	
46	Unknown Trib to Ganga	25.502	86.481	42	1.64	21.7	1.0	2.31
47	Inundated Area	25.406	86.779	36	1.09	20.2	0.6	
48	Kosi	25.424	87.235	31	1.58	24.6	0.4	9.34
49	Ganga	25.282	87.248	40	2.23	20.9	0.2	
50	Ganga	24.801	87.948	27	1.66	22.1	0.1	
51	Hooghly	22.651	88.351	7	1.66	20.6	0.3	

952

953 Table 1. Dissolved load Li isotope ratios and silicate weathering rates. See Frings

954 et al. (2015) for major and trace element concentrations. “2sd” refers to the 2

955 standard deviations of multiple analyses of the same solution (generally n=3).

956

Sample	Position	Depth (m)	$\delta^7\text{Li}$	2sd
1	Surface	0	-1.6	0.1
2	Surface	0	0.1	0.1
14	Bank		0.2	0.1
28	Shallow	0	-0.6	0.6
28	Deep	-	-1.3	0.7

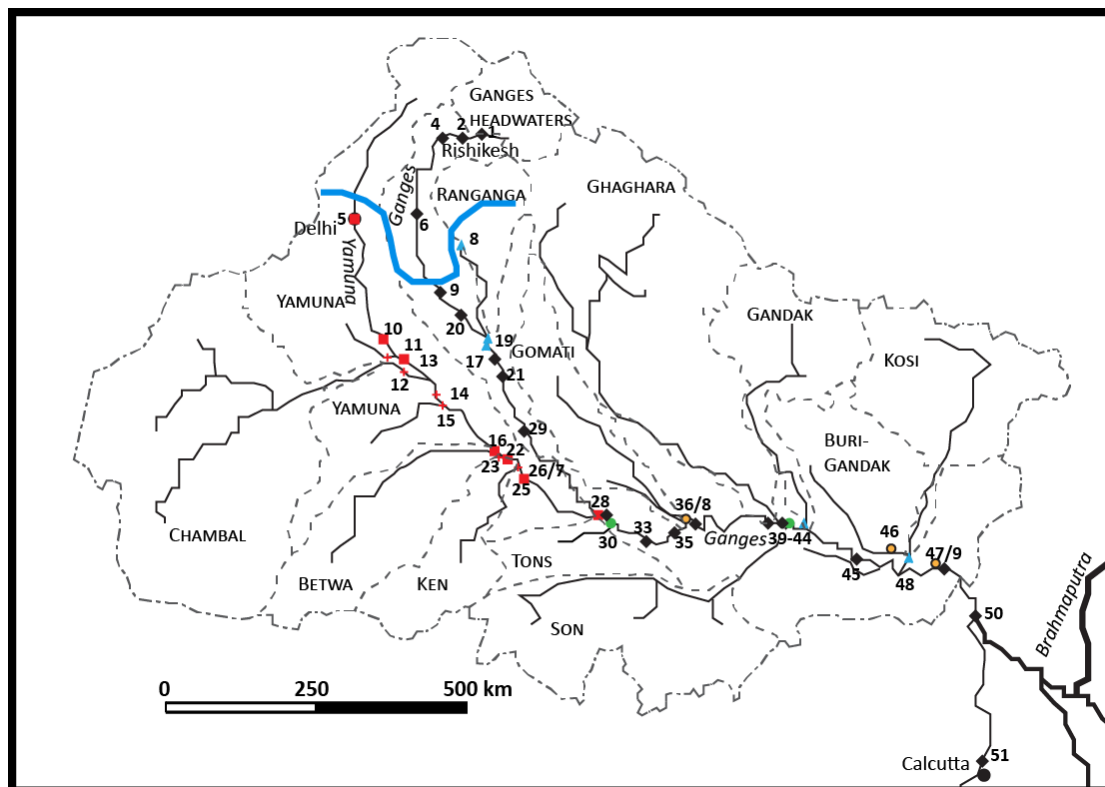
40	Shallow	0	-2.6	0.6
40	Deep	3	2.9	0.6
41	Shallow	0	-0.1	0.6
41	Medium	5	0.1	0.6
41	Deep	9	0.0	0.5
49	Shallow	0	-0.4	0.2
49	Deep	10	0.1	0.2

957

958 Table 2. Sediment Li isotope ratios. Sample locations are the same as for Table 1.

959

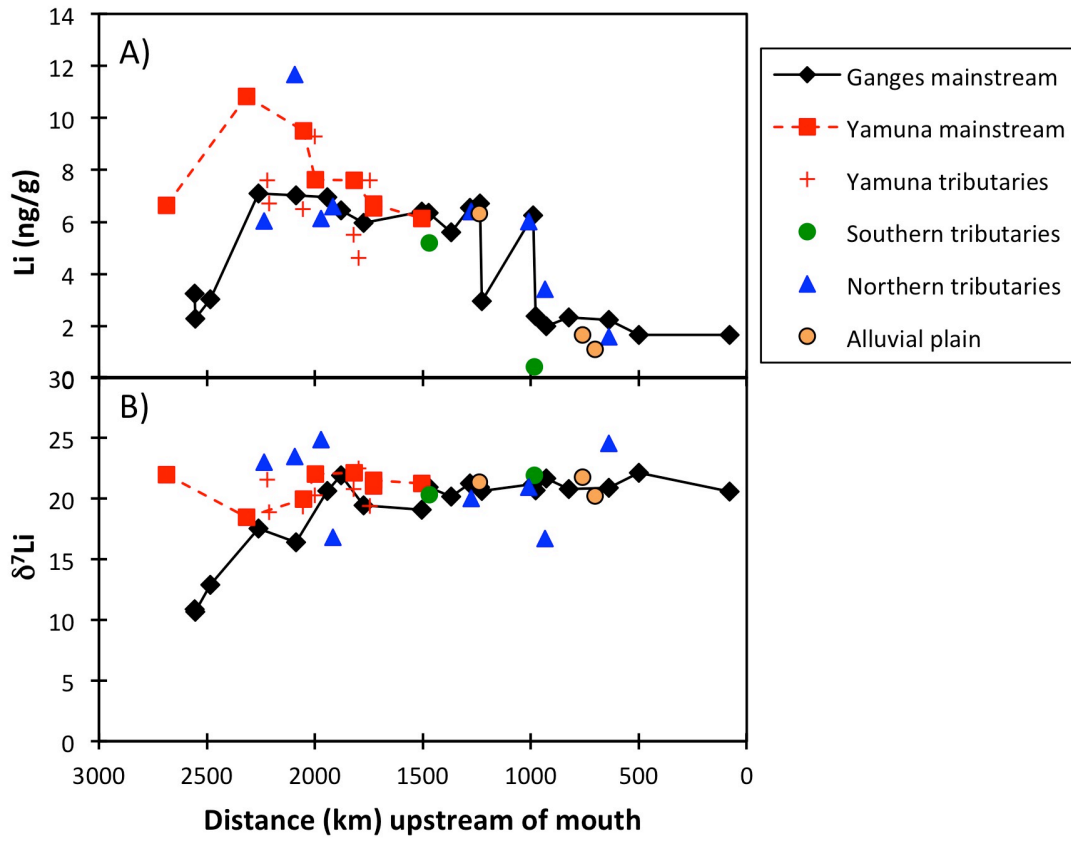
960



961

962 Figure 1. Sample location map, modified from Frings et al. (2015). The dotted  
 963 grey lines show the individual catchment areas. The sample location symbols are  
 964 the same as those used in Figures 2 and 8. The blue curved line shows the  
 965 location below which the floodplain is at steady-state according to dissolved Li  
 966 isotopes (see text for details).

967

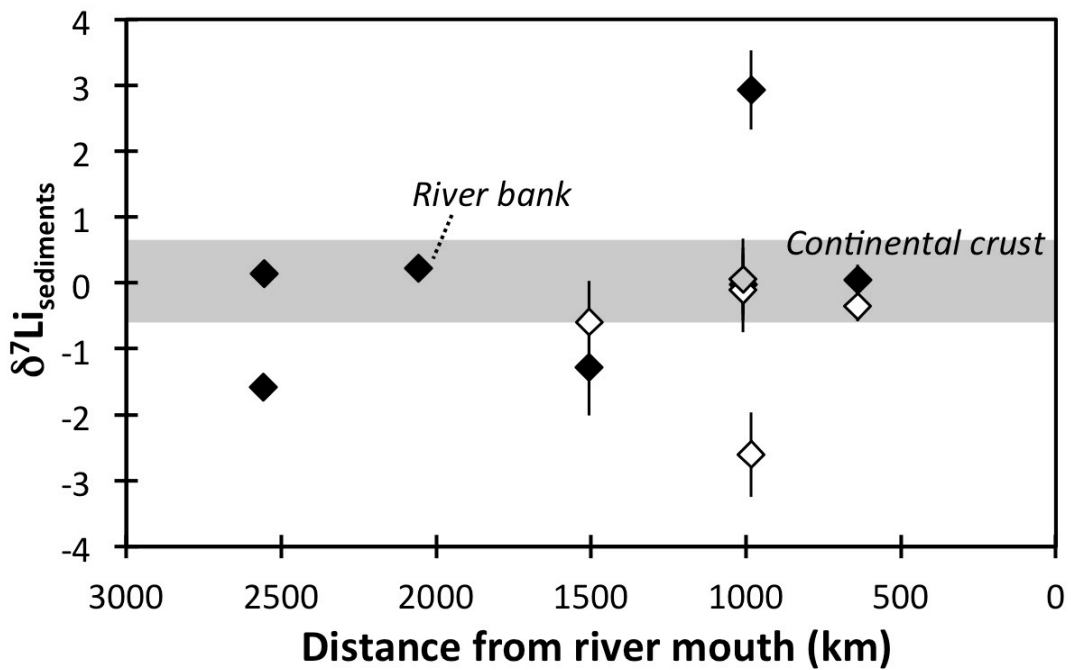


968

969 Figure 2. Comparison of the Li concentration (A) and isotope ratio (B) to flow

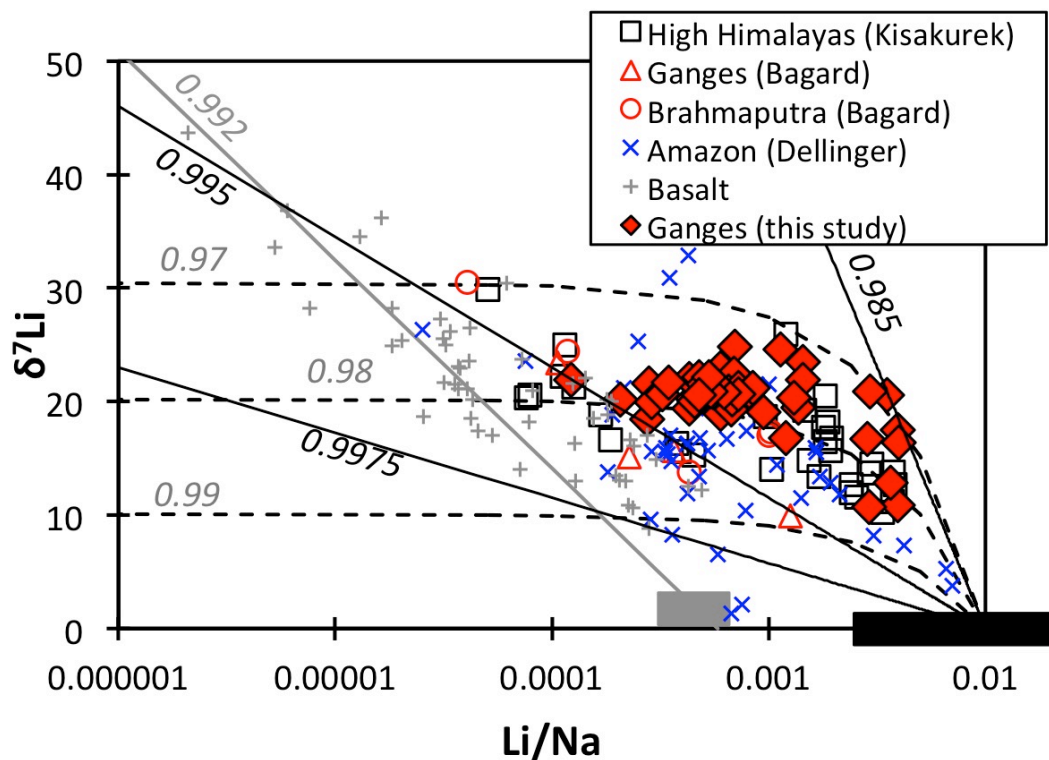
970 distance upstream from the river mouth for the Ganges and its tributaries.

971



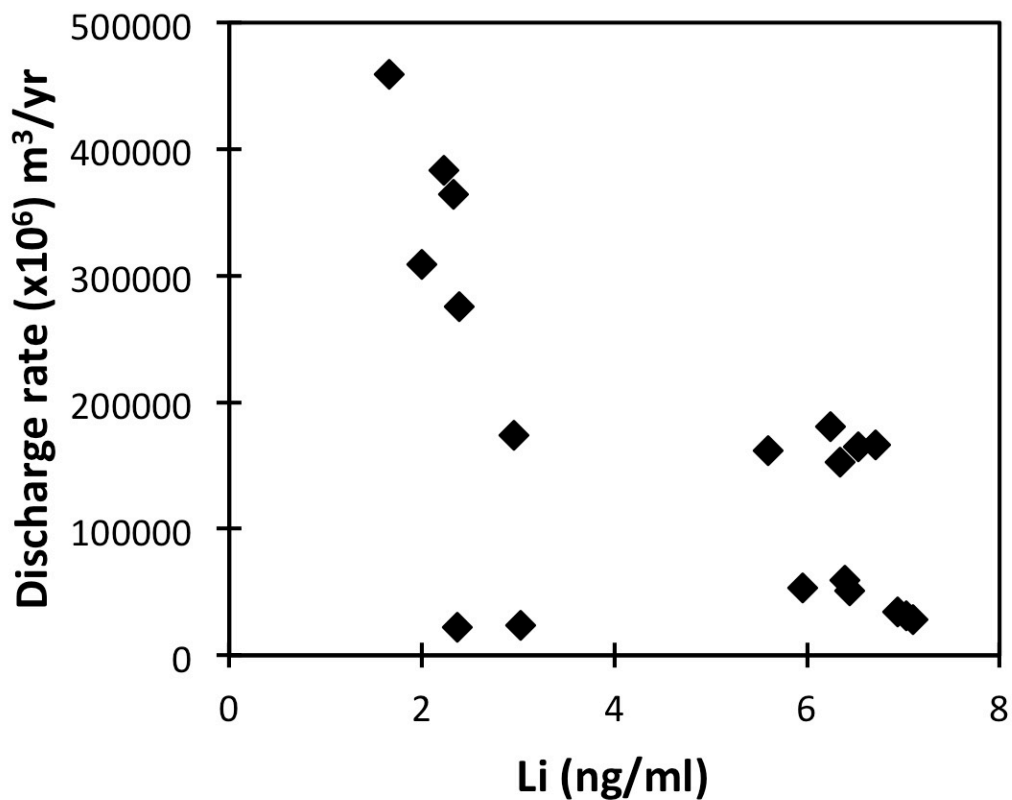
972

973 Figure 3. Li isotope ratio of river sediments plotted as a function of flow distance  
 974 above the river mouth. Open diamonds are shallow samples from the river flow,  
 975 filled grey symbol is medium depth, and black symbols are deeper samples. The  
 976 grey bar is the mean continental crust (Sauzeat et al., 2015).  
 977

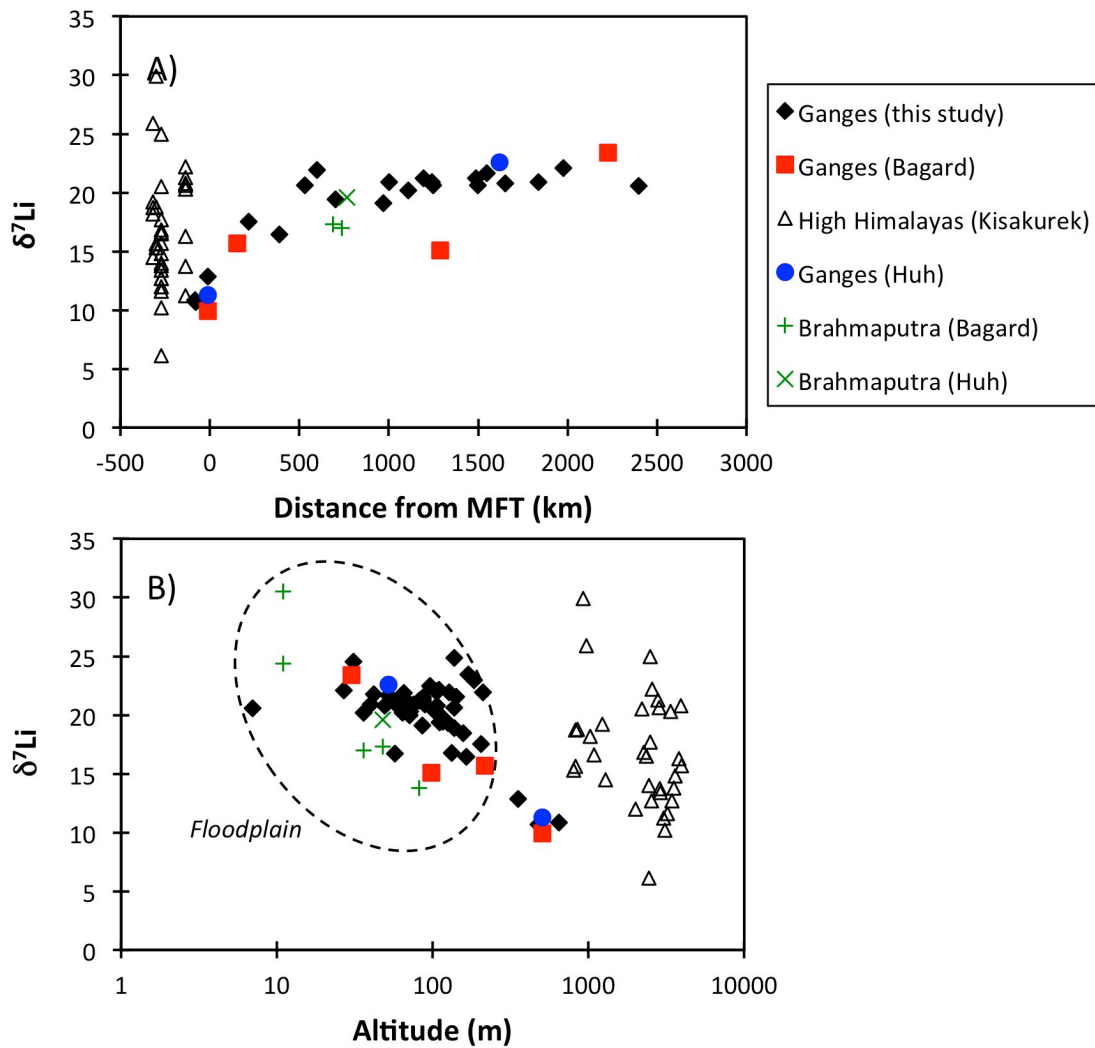


978  
 979 Figure 4. Dissolved Li/Na mass ratios plotted against  $\delta^7\text{Li}$  for this study, the High  
 980 Himalayas (Kisakürek et al., 2005), the Ganges-Brahmaputra (Bagard et al.,  
 981 2015), the Amazon (Dellinger et al., 2015) and basalts from Iceland, the Azores  
 982 and the Columbia River Basalts (Liu et al., 2015; Pogge von Strandmann et al.,  
 983 2010; Pogge von Strandmann et al., 2006; Vigier et al., 2009). The solid lines are  
 984 Rayleigh fractionation relationships (see text for details), the dashed lines are  
 985 Batch fractionation relationships and the associated numbers the isotopic  
 986 fractionation factors (black for Rayleigh, grey for Batch). The black box

987 represents the range of Li/Na from river sediments from the Amazon and  
988 Ganges, as well as global shales (Dellinger et al., 2014). The grey line is a Rayleigh  
989 relationship for basaltic terrains, using the grey box as a starting composition  
990 (Pogge von Strandmann et al., 2010; Pogge von Strandmann et al., 2006).  
991 Dissolved load values have been corrected for precipitation input when data  
992 have been provided, otherwise are uncorrected.  
993



994  
995 Figure 5. Li concentrations plotted against discharge rates. Samples are  
996 unaffected by dilution, except potentially those with highest discharge, which are  
997 those close to the Ganges mouth and have constant  $\delta^7\text{Li}$ .  
998



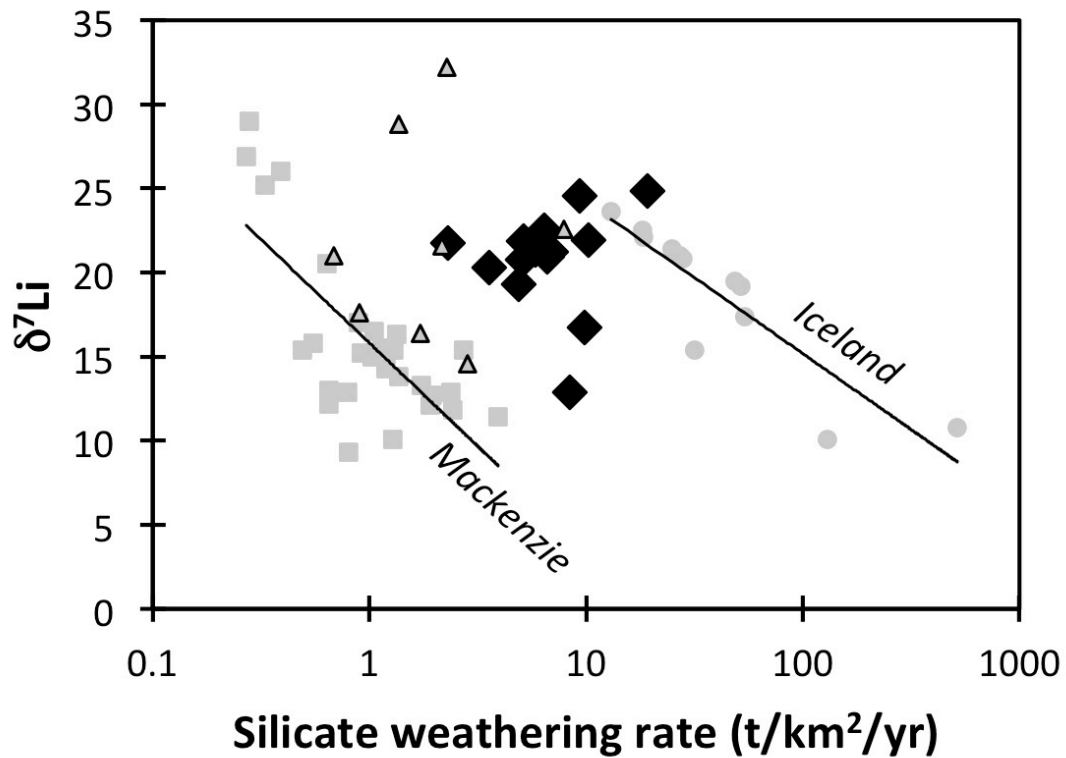
999

1000 Figure 6. A) Dissolved Li isotope ratios for all studies of the Ganges-Brahmaputra  
 1001 rivers system, plotted against distance from the Main Frontal Thrust (MFT) that  
 1002 delineates the edge of the high relief areas (Bagard et al., 2015; Huh et al., 1998;  
 1003 Kisakürek et al., 2005), showing the unchanging nature of  $\delta^7\text{Li}$  in the Ganges over  
 1004 at least 3 decades. Only rivers that actually cross the MFT are plotted. Distances  
 1005 for the Kisakurek et al. (2005) rivers were measured using Google Maps. B) The  
 1006 same data plotted against altitude, as an approximation of uplift and exposure  
 1007 rates. Samples from south of the MFT are considered floodplain samples.

1008

1009





1010

1011 Figure 7. Riverine Li isotopes plotted as a function of the silicate weathering rate.

1012 While there are correlations between the two parameters for two relatively

1013 small river systems (Iceland and the Mackenzie River (Milot et al., 2010; Vigier

1014 et al., 2009)), there is not correlation for large global rivers (triangles (Huh et al.,

1015 1998)), or for the Ganges (this study – black diamonds) which are responsible

1016 for >30% of the global riverine discharge into the oceans. Lithium isotopes are

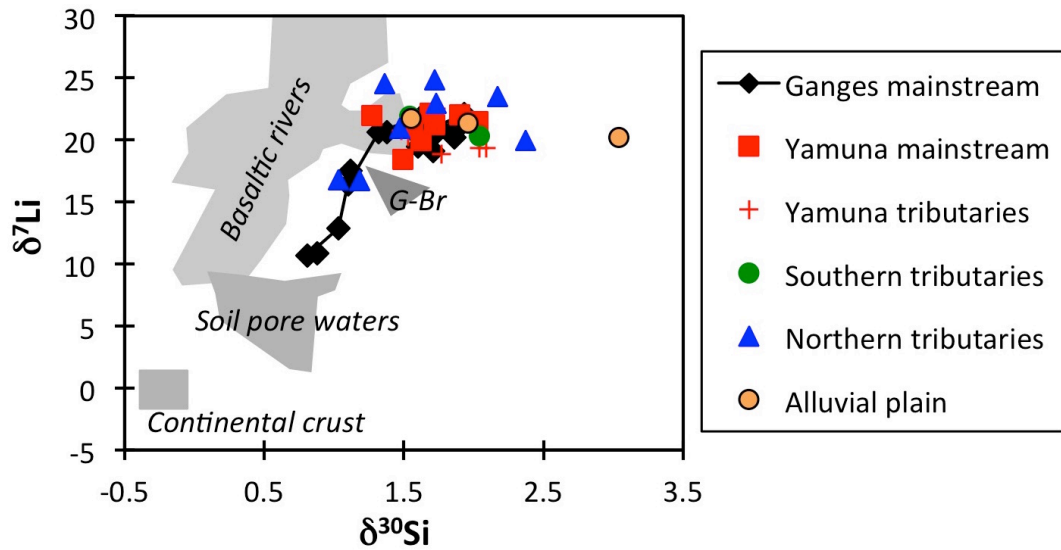
1017 therefore clearly not a weathering-rate tracer, and cannot be used as such in the

1018 palaeo-record.

1019

1020

1021



1022

1023 Figure 8. Li isotopes plotted against Si isotopes (Frings et al., 2015) for the  
 1024 Ganges river system. The Ganges mainstream exhibits a positive correlation,  
 1025 which most other samples do not. In comparison, a few points from a previous  
 1026 Ganges-Brahmaputra (G-Br) study are shown (Bagard et al., 2015; Georg et al.,  
 1027 2009). Some basaltic rivers also exhibit a Li-Si co-variation (Opfergelt et al.,  
 1028 2013), while neither some other Icelandic rivers (Georg et al., 2007; Vigier et al.,  
 1029 2009), nor Icelandic soil pore waters exhibit a co-variation (Pogge von  
 1030 Strandmann et al., 2012). Average upper continental crust values are from  
 1031 Sauzeat et al., 2015; Savage et al., 2010.

1032

1033

1034